

See discussions, stats, and author profiles for this publication at: <https://www.researchgate.net/publication/26807013>

Design, synthesis, and X-ray crystal structures of 2,4-diaminofuro[2,3-d]pyrimidines as multireceptor tyrosine kinase and dihydrofolate reductase inhibitors

ARTICLE *in* BIOORGANIC & MEDICINAL CHEMISTRY · AUGUST 2009

Impact Factor: 2.79 · DOI: 10.1016/j.bmc.2009.08.044 · Source: PubMed

CITATIONS

13

READS

28

10 AUTHORS, INCLUDING:



Aleem Gangjee

Duquesne University

202 PUBLICATIONS 2,829 CITATIONS

[SEE PROFILE](#)



Michael A Ihnat

University of Oklahoma Health Sciences Center

72 PUBLICATIONS 1,989 CITATIONS

[SEE PROFILE](#)



Vivian Cody

University at Buffalo, The State University of...

131 PUBLICATIONS 2,342 CITATIONS

[SEE PROFILE](#)



Sherry F Queener

Indiana University-Purdue University Indiana...

226 PUBLICATIONS 4,801 CITATIONS

[SEE PROFILE](#)



NIH Public Access

Author Manuscript

Bioorg Med Chem. Author manuscript; available in PMC 2010 October 15.

Published in final edited form as:

Bioorg Med Chem. 2009 October 15; 17(20): 7324–7336. doi:10.1016/j.bmc.2009.08.044.

Design, Synthesis, and X-ray Crystal Structures of 2,4-Diaminofuro[2,3-*d*]pyrimidines as Multireceptor Tyrosine Kinase and Dihydrofolate Reductase Inhibitors

Aleem Gangjee ^{*, Wei Li[†], Lu Lin[†], Yibin Zeng[†], Michael Ihnat[‡], Linda A. Warnke[‡], Dixy W. Green[‡], Vivian Cody[§], Jim Pace[§], and Sherry F. Queener^{||}}

[†]Division of Medicinal Chemistry, Graduate School of Pharmaceutical Sciences, Duquesne University, 600 Forbes Avenue, Pittsburgh, Pennsylvania 15282

[‡]Department of Cell Biology, The University of Oklahoma Health Science Center, Oklahoma City, Oklahoma 73104

[§]Hauptman-Woodward Medical Research Institute, Inc., 700 Ellicott St., Buffalo, New York 14203

^{||}Department of Pharmacology and Toxicology, School of Medicine, Indiana University, Indianapolis, Indiana 46202

Abstract

To optimize dual receptor tyrosine kinase (RTK) and dihydrofolate reductase (DHFR) inhibition, the E- and Z-isomers of 5-[2-(2-methoxyphenyl)prop-1-en-1-yl]furo[2,3-*d*]pyrimidine-2,4-diamines (**1a** and **1b**) were separated by HPLC and the X-ray crystal structures (2.0 Å and 1.4 Å respectively) with mouse DHFR and NADPH as well as **1b** with human DHFR (1.5 Å) were determined. The E- and Z-isomers adopt different binding modes when bound to mouse DHFR. A series of 2,4-diaminofuro[2,3-*d*]pyrimidines **2–13** were designed and synthesized using the X-ray crystal structures of **1a** and **1b** with DHFR to increase their DHFR inhibitory activity. Wittig reactions of appropriate 2-methoxyphenyl ketones with 2,4-diamino-6-chloromethyl furo[2,3-*d*]pyrimidine afforded the C8–C9 unsaturated compounds **2–7** and catalytic reduction gave the saturated **8–13**. Homologation of the C9-methyl analog maintains DHFR inhibitory activity. In addition, inhibition of EGFR and PDGFR-β were discovered for saturated C9-homologated analogs **9** and **10** that were absent in the saturated C9-methyl analogs.

Keywords

PDGFR-β; EGFR; Dihydrofolate reductase; Multitargeted inhibitors

© 2009 Elsevier Ltd. All rights reserved.

*To whom correspondence should be addressed. Phone: 412-396-6070. Fax: 412-396-5593. gangjee@duq.edu.

Publisher's Disclaimer: This is a PDF file of an unedited manuscript that has been accepted for publication. As a service to our customers we are providing this early version of the manuscript. The manuscript will undergo copyediting, typesetting, and review of the resulting proof before it is published in its final citable form. Please note that during the production process errors may be discovered which could affect the content, and all legal disclaimers that apply to the journal pertain.

Supporting Information Available:

Elemental Analysis and High-Resolution Mass Spectra (HRMS) (EI) and HPLC separation. This material is available free of charge via the Internet at <http://pubs.acs.org>.

Introduction

Angiogenesis, the formation of new blood vessels from pre-existing vasculature, plays a crucial role in the growth and metastasis of solid tumors.¹ Angiogenesis and metastasis contribute to the poor prognosis in patients with angiogenic solid tumors.² In addition, angiogenesis has been considered the key step in the transformation of some tumor cells from the dormant state to the malignant state. Thus, inhibition of tumor angiogenesis is an attractive target for the development of new antitumor agents.^{3, 4}

Some of the receptors⁵ involved in angiogenesis are members of the receptor tyrosine kinase (RTK) superfamily, which includes vascular endothelial growth factor receptor (VEGFR), epidermal growth factor receptor (EGFR), platelet-derived growth factor receptor (PDGFR), and fibroblast growth factor receptor (FGFR) among several others.⁶ These RTKs have been implicated in the development, progression, and aggressiveness and metastasis of a variety of solid tumors including head and neck cancers,⁷ non-small cell lung cancer^{8, 9} and glioblastomas.^{10, 11} These RTKs promote signal transduction via autophosphorylation that results in angiogenesis.^{12–17}

Thus, RTKs are attractive targets for the development of cancer chemotherapeutic agents.^{18, 19} Several small molecule inhibitors of RTKs that are directed at the ATP site are currently used clinically and several are in clinical trials as antitumor agents²⁰ (Figure 1).

Erlotinib and gefitinib inhibit EGFR that is overexpressed in tumors, and are approved antitumor agents.²¹

VEGF and its receptor VEGFR-2 play crucial roles in vessel sprouting and new vessel initiation in early stages of angiogenesis.²² Inhibition of VEGFR-2 affords excellent antitumor agents.²² Platelet-derived growth factor receptor (PDGFR) kinases also directly contribute to tumor growth by modifying the tumor microenvironment.²³

The first generation of therapeutic antiangiogenic agents were designed to selectively inhibit specific RTKs, but angiogenesis mechanisms can often be carried out by more than one RTK. Simultaneous targeting of two or more RTKs has recently emerged as a more advantageous strategy that may circumvent resistance that develops with inhibitors aimed at a single RTK.²⁰ The recently approved inhibitors of multiple RTKs, sunitinib and sorafenib, are examples of anticancer agents exploiting this strategy.

Dihydrofolate reductase (DHFR) is an enzyme that catalyzes the reduction of dihydrofolate to tetrahydrofolate and provides the precursor for the folate cofactors that transfer one carbon units in the synthesis of metabolites, including purines and pyrimidines. Inhibition of DHFR blocks DNA synthesis among other metabolic pathways and causes cell death. Thus DHFR inhibitors such as methotrexate (MTX) (Figure 1) and the multitargeted folate metabolizing enzyme inhibitor, pemetrexed (PMX) (Figure 1), are clinically used antitumor agents. A variety of classical antifolates (with the L-glutamate as in MTX and PMX) and nonclassical antifolates (with lipophilic aryl side chains) like piritrexim (PTX) (Figure 1) and trimetrexate (TMQ) (Figure 1) have been used as cytotoxic agents in trials for cancer treatment. The structure of these agents usually contain a pyrimidine ring that is substituted in the 2- and 4-positions with amino groups. This 2,4-diaminopyrimidine is usually fused to a second ring which contains a substitution in the 5- or 6-position. Several comprehensive structure-activity reviews of DHFR inhibitors are available in the literature.^{24–26} X-ray crystal structures of DHFR with 2,4-diamino substituted fused pyrimidine rings demonstrate that this fused 2,4-diaminopyrimidine ring is protonated at physiological pHs and forms an ionic bond with a conserved glutamate or aspartate (Glu30 in hDHFR).²⁷ X-ray crystal structures show that the fused pyrimidine ring

of these 2,4-diamino analogs is rotated 180° compared to that of folate when bound to DHFR.
27

RTK inhibitors and antiangiogenic agents are generally cytostatic and the combinations of such agents with standard cytotoxic chemotherapeutic agents, including antifolates such as MTX and PMX among others significantly improves clinical response in trials. We proposed to combine RTK inhibitory activity (cytostatic) with DHFR inhibitory activity (cytotoxic) in a single molecule to gain several advantages. The dual targets of RTKs and DHFR should retard development of resistance and single molecules simplify the pharmacokinetics and toxicity issues compared to two or more separate agents. Our initial attempt at providing both cytostatic activity (via RTK inhibition) and cytotoxic or tumorcidal activity (via DHFR inhibition) in single molecules involved 5-substituted 2,4-diaminofuro[2,3-*d*]pyrimidines including the E-isomer **1a** and the Z-isomer **1b** 28 (Figure 2). These compounds demonstrated excellent dual RTK inhibitory activities (VEGFR-2 and PDGFR- β) along with modest DHFR inhibition. In addition, some of the analogs demonstrated tumor growth inhibition and a decrease of tumor lung metastases in a mouse model of B16 melanomas.²⁸

The first objective of the present study was to separate and individually evaluate the E- and Z-isomers, **1a** and **1b** respectively, to ascertain and compare the influence of the geometric isomers on biological activities. Molecular modeling in the previous report²⁸ predicted two different modes of binding of **1a** and **1b** to DHFR. Thus, the second objective of this study was to determine the X-ray crystal structures of the separated E- and Z-isomers **1a** and **1b** respectively with DHFR. Finally, the RTK inhibitory activity of the previous compounds compared to standards was very good, but the DHFR inhibitory activity was marginal. On the basis of molecular modeling we determined that the 9-CH₃ group of the previous analogs (specifically **1b**) and Val115 of human DHFR were too distant to interact. Hence, a third objective of this study was to increase DHFR inhibitory effects of the parent 9-CH₃ compounds via homologation of the 9-CH₃ moiety to afford **2–7** (Figure 3) a propyl, isopropyl, cyclopropyl, butyl, isobutyl and a sec-butyl respectively, to provide hydrophobic (van der Waals) interactions with Val115 of hDHFR. It was also necessary to maintain or improve the RTK inhibitory activities. Molecular modeling of **2–7** using the published X-ray crystal structure of VEGFR-2 and a sequence homology alignment with the X-ray crystal structure of insulin receptor kinase containing a bound ATP molecule as we reported previously,²⁸ allowed the superimposition of energy minimized conformations of **2–7** on ATP in VEGFR-2. This indicated that there was sufficient space in the area around the R substituent of **2–7** to allow the C9-alkyl moiety to interact with Cys1045 and Val848 in the Z- and E-isomers and hence allow activity in VEGFR-2. Since there is no X-ray crystal structure of PDGFR- β available, homology modeling suggested that the R substituent in **2–7** should maintain PDGFR- β activity. In addition, it was also of interest to evaluate the corresponding saturated analogs **8–13** (Figure 3) to determine the contribution, if any, of the C8–C9 double bond and its restricted conformation to the biological activities (RTK inhibition and DHFR inhibition).

HPLC separation and isolation of the Z-isomer **1b**

We obtained the pure E-isomer **1a** through silica gel chromatography.²⁸ Purification of the Z-isomer **1b** required reverse phase HPLC (Waters® 4000 system equipped with an X-Bridge® C-18 19 × 50 mm column, Waters® 2487 Dual λ Absorbance Detector). Multiple variations of conditions were evaluated, including both isocratic and gradient mobile phase compositions. The solvent system with 75% water and 25% acetonitrile (for 0–1 min, 10 mL/min; for 1 min and beyond, 35 mL/min) was found to be the most efficient. Retention times for the Z- and E-isomers are 6.580 min and 11.453 min respectively. Purity was confirmed by the same reverse phase HPLC system.

Confirmation of the separation of the E- and Z-isomers by ^1H NMR

In the ^1H NMR, the 6-H of the Z-isomer of the furo[2,3-*d*]pyrimidine ring occurs at δ 6.06, due to a shielding effect of the phenyl ring, which is significantly different from the 6-H of the E-isomers, at δ 7.47²⁴ where there is no shielding of the phenyl ring.

X-ray Crystal Structure

Structural data for the inhibitors **1a** and **1b** in complex with NADPH and mouse (m) DHFR, as well as inhibitor **1b** with human (h) DHFR, were determined to validate the binding orientation of these isomers in the active site of DHFR. As illustrated in Figure 4 (below), the binding of the E-isomer **1a** is observed in a “flipped” mode in mDHFR such that the furo oxygen of the furo[2,3-*d*]pyrimidine of **1a** occupies the 4-amino position of 2,4-diaminopyrimidine antifolates such as MTX,^{27, 29} and also as observed for the Z-isomer, **1b** for hDHFR and mDHFR (Figure 5). Compound **1a** is the first example of a furo[2,3-*d*]pyrimidine antifolate binding in a “flipped” orientation.

The overall structure of the ternary mDHFR and hDHFR complexes with NADPH and **1a** or **1b** are similar to previously reported structures.^{30, 31} The furo[2,3-*d*]pyrimidine ring in the E-isomer **1a** binds with the 2-amino and N3 of the pyrimidine interacting via hydrogen bonds with Glu30 (Figure 6), and is similar to that observed for folic acid (FA). In this orientation the 7-oxo group of the furo[2,3-*d*]pyrimidine of **1a** interacts with the backbone functional groups of Ile7, Val115, the hydroxyl of Tyr121, and the nicotinamide carboxamide group of NADPH.³² Similar to the MTX binding mode,³⁰ the 4-amino group of the Z-isomer **1b** makes a number of hydrogen bonding interactions with the backbone functional groups of Ile7 (3.0 Å) and Val115 (2.9 Å) and the side chains of Tyr121 (3.4 Å) and the nicotinamide of NADPH (3.7 Å) that contribute to the tight binding of antifolates.³⁰ The Z-isomer **1b** places the 2-methoxyphenyl ring cis to the furo[2,3-*d*]pyrimidine ring. In this orientation, the 9-methyl and the 2'-methoxy methyl make van der Waals contacts with the methyl of Thr56 (3.6 Å and 3.8 Å, respectively). On the other hand, in the “flipped” orientation, the furo oxygen of **1a** makes much weaker contacts to Ile7 (3.2 Å), Val115 (3.4 Å), Tyr121 (3.4 Å) and the nicotinamide of NADPH (3.7 Å). The 9-methyl and 2'-methoxy methyl contacts with Thr56 are 3.9 Å and 4.6 Å, respectively. The 4-amino group of the E-isomer **1a** interacts with a water molecule but does not make close contact to Glu30.

Inspection of the electron density profile for the inhibitor further reveals that the configuration about the bridging double bond places the 9-methyl group in the *E*-configuration (the methyl group is cis and coplanar with the furo ring system (Figure 4 and Figure 5). In both the E-isomer **1a** and Z-isomer **1b** mDHFR and hDHFR structure, the C9-methyl and the 2'-methoxyphenyl group occupy the same position in the active site of mouse DHFR (Figure 7 and Figure 8).

In fact, modeling studies show that if either **1a** or **1b** were to bind with the alternate furo[2,3-*d*]pyrimidine orientation, that is if either molecule were to be rotated by 180° about the C2-NH₂ bond, then the 2'-methoxyphenyl ring would make unfavorable contacts to residues Thr56, Ile60 and Leu67 in the active site. These data demonstrate the influence of conformational flexibility of DHFR in adapting different binding modes in the active site. In addition, these results indicated that both mDHFR and hDHFR show a slight but not statistically significant preference for the Z-isomer within the active site binding pocket.

On the basis of molecular modeling Gangjee et al.²⁸ had predicted that the Z-isomers of these furo[2,3-*d*]pyrimidines could bind in the normal mode and the E-isomers could bind in the flipped mode. The X-ray crystal studies of the individual E- and Z-isomers do indeed confirm the predicted orientations of the E- and Z-isomer binding to DHFR.

Molecular modeling

Molecular modeling using SYBYL 8.0³⁴ and superimposition of the E-isomer **3** (Figure 3) on **1a** crystallized with mDHFR indicated that, like compound **1a**, the E-isomer of **3** can bind in the mDHFR binding pocket with a “flipped” orientation (Figure 9) such that the furo oxygen of the furo[2,3-*d*]pyrimidine occupies the 4-amino position observed in the binding of 2,4-diaminopyrimidine antifolates like MTX.³⁰ In addition, the C-9 isopropyl moiety of the E-isomer of **3** makes hydrophobic contact with Val115 as does the C-9 methyl moiety of **1a**. The van der Waals distance of the methyl of the C9-isopropyl group of E-**3** from Val115 is 3.48 Å and 4.10 Å for the methyl and methylene of Val115 respectively, which is much closer than that for the C9-methyl group of **1a** and was expected to improve the hDHFR inhibitory activity. The other methyl group of the C9-isopropyl moiety of E-**3** interacts with the methyl and methylene groups of Ile60 as shown in Figure 9.

Similarly, molecular modeling (SYBYL 8.0) and superimposition of the Z-isomer of **3** onto **1b** in the mDHFR X-ray crystal structure showed that like **1b**, the Z-isomer of **3** could also bind with mDHFR using the “normal” 2,4-diaminopyrimidine ring binding geometry with the furo oxygen of the furo[2,3-*d*]pyrimidine near Glu30 and the 4-amino interacting near the cofactor nicotinamide ring (Figure 10).

In addition, the C9-isopropyl moiety of the Z-isomer of **3** makes better hydrophobic contact with Val115 than the C9-methyl moiety of **1b**. The van der Waals distance from one of the methyl moieties of the C9-isopropyl group of the Z-isomer **3** to the methyl and methylene of Val115 is 3.45 Å and 3.72 Å respectively (Figure 10), which is much closer than that for the C9-methyl group of **1b**. In addition the other methyl group of the C9-isopropyl moiety of Z-**3** interacts with Ile60 at 3.53 Å (Figure 10). Thus, it was anticipated that both the E- and Z-isomers of **3** would have better DHFR inhibitory activity compared to **1a** and **1b**. Further molecular modeling also indicated that larger alkyl substitutions such as cyclopropyl, n-butyl, isobutyl, sec-butyl could also be accommodated into this binding pocket at the C9-position. These molecular modeling studies afford credence to our original hypothesis that homologating the 9-CH₃ moiety should increase hDHFR inhibition.

Chemistry

The previously described method²⁸ was modified for the synthesis of 5-(chloromethyl)furo[2,3-*d*]pyrimidine-2,4-diamine, **16** (Scheme 1). Reaction of **16** with the corresponding ketones using Wittig type condensations under basic conditions afforded the desired target compounds **2–7**. The required alkyl 2-methoxyphenyl ketones were synthesized according to literature methods.^{35–38} The crucial intermediate, 5-(chloromethyl)furo[2,3-*d*]pyrimidine-2,4-diamine **16**, was readily obtained by the condensation of 2,6-diaminopyrimidin-4-ol **14** and 1,3-dichloroacetone **15** in DMF at room temperature.³⁹ Displacement of the chloride with tributylphosphine followed by NaH in anhydrous DMSO afforded the semistable ylide. This ylide was immediately reacted with the appropriate ketone to afford the desired olefinic compounds **2–7** in 18–45% yield usually as mixtures of E- and Z-isomers. The yields of the Wittig reaction were lower than those reported²⁸ for the lead compounds **1a** and **1b**. The reason for the lower yields is probably the steric effect of the larger 9-substitution. Final compounds **2–7** were E/Z-mixtures which were difficult to separate using flash or column chromatography. Hydrogenation of compounds **2–7** in CH₃OH/CHCl₃ afforded the desired reduced compounds **8–13** as racemic mixtures with yields that varied from 35 to 65 %.

Biological Evaluation and Discussion

Kinase activity of the compounds **1b** and **2–13** were evaluated using human tumor cells known to express high levels of VEGFR-2 (Flk-1, KDR), EGFR, and PDGFR-β using a

phosphotyrosine ELISA.^{40, 41} The effect of the compounds on cell proliferation was measured using A431 human epithelial carcinoma cells that overexpress EGFR. Finally, the effect of selected compounds on blood vessel formation was assessed using the chicken embryo chorioallantoic membrane (CAM) assay, a standard test for angiogenesis.⁴² All the experimental methods for evaluation were as previously described by Gangjee et al.⁴³ Since the IC₅₀ values of the same compound vary under different assay conditions, we used a standard (control) compound in each of the evaluations to provide a valid comparison with the synthesized analogs. For VEGFR-2 the standard was semaxanib (Figure 1); for EGFR the standard was **17** (PD153035, Figure 1); for PDGFR- β the standard was 6,7-dimethyl-2-phenyl quinoxaline (Figure 1, AG1295) **18**; for the cytotoxicity study against the growth of A431 cells in culture the standard was **17**. Semaxanib was also used as the standard for the CAM assay.

As shown in Table 1 the *E*-isomer **1a** was more potent in all of the assays listed compared to the *Z*-isomer **1b**, thus indicating that the *E*-configuration is preferred for RTK inhibition. In the EGFR assay (Table 1), most of the unsaturated compounds **2–7** were inactive. In contrast to the previous report of the C9-methyl analogs,²⁸ the saturated analogs of the homologated series (**8–11**) demonstrated good inhibitory activity against EGFR. Among these compounds the propyl analog **8**, showed an IC₅₀ value significantly better than **1a** and only 9-fold less than the standard **17**. A moderate EGFR inhibitory activity was obtained for **9** and **11** (Table 1). Most of the side chain saturated analogs were more potent than the unsaturated analogs. These results indicate that the restricted C8=C9 conformation is not conducive to potent EGFR inhibitory activity and depends more on the size of the C9-alkyl substitution. Against VEGFR-2 the most potent compound was **13**, which was similar to the parent **1a** and 7-fold less than the standard VEGFR-2 inhibitor semaxanib. Among the side chain unsaturated analogs, increasing the chain length or bulk at the C9-position beyond a propyl drastically reduced VEGFR-2 inhibitory activity.

Compound **2** maintained PDGFR- β activity, similar to **1a**, and improved hDHFR inhibitory activity compared to **1a** but is about 7-fold less potent against VEGFR-2. However, except for **2**, these C9-homologated unsaturated analogs lost their activity against PDGFR- β and VEGFR-2 compared to **1a** and **1b**. On the basis of the data against both VEGFR-2 and PDGFR- β increasing the size and/or length of the C9-alkyl substitution beyond propyl is detrimental to RTK inhibitory activity for the unsaturated analogs. In the PDGFR- β inhibitory assay, saturated compound **9** was more potent than the standard compound **18** and compounds **2** and **10** were similar to the standard **18** and the parent analog **1a**. The trend indicated that increasing the chain length or bulk at C9 beyond an isopropyl was detrimental to PDGFR- β activity.

Cytotoxicity studies against the growth of A431 tumor cells in culture that overexpress EGFR compared analogs **2–13** with standard compounds **17** and semaxanib. The most potent compound was the unsaturated C9-cyclopropyl **4**, which was somewhat more active than the standards. Compounds **6**, **7** and **12** were similar to **17** and semaxanib. The other analogs were much less active than the standard compounds. For compounds **2–13** there was no correlation of the EGFR inhibitory activity with cytotoxicity against A431 cells in culture. A possible explanation for the lack of correlation is that transport and/or other factors such as DHFR inhibition (see below) may influence the cytotoxic activity against A431 cells in culture. In the CAM assay, none of these compounds **2–13** were more potent than lead compound **1a** or the standard semaxanib.

Compounds **1a**, **1b** and **2–13** were also evaluated as inhibitors of mammalian DHFR (human (h), rat liver (rl), and mouse (m)), and of *Pneumocystis carinii* (Pc) DHFR, and *Toxoplasma gondii* (Tg) DHFR (Table 2). Against hDHFR, rlDHFR and mDHFR the IC₅₀ values of the analogs showed a similar trend. Among the unsaturated analogs **2–4** and **7** were most potent against the mammalian DHFRs, but these compounds were not consistently active against

PcDHFR and TgDHFR; compounds **3**, **4** and **7** were active against TgDHFR but not against PcDHFR. Since the only variation in these analogs is the alkyl C9-substituent clearly this moiety dictates both the potency and the selectivity for DHFR in this series.

Among the reduced analogs **8–13** only compounds **9** and **10** showed consistently potent inhibition of mammalian DHFR; neither of these compounds was a strong inhibitor of PcDHFR but they did inhibit TgDHFR. The similar activity of the **3** and **9** pair as well as the **4** and **10** pair argues that for some of these C9-alkyl substituted compounds conformational restriction about the C8–C9 bond did not play a major role in the inhibitory activity against DHFR. In other cases, conformational restriction about the C8–C9 bond clearly did play a role; for example in mDHFR a 20-fold decrease in inhibition is observed on reduction of **2** to **8** and a 6-fold decrease is observed on reduction of **5** to **11**.

The saturated compounds also showed some dependence on the alkyl C9-substituent for potency and selectivity for PcDHFR and TgDHFR, but none of the compounds were appreciably potent or selective against these non-mammalian DHFR.

The hDHFR inhibitory activity also has an effect on A431 cytotoxicity. Thus for **4** and **7** there is a direct correlation of the hDHFR inhibitory activity (Table 2) and the A431 cytotoxicity (Table 1). Unfortunately the other analogs do not show this correlation.

In order to more carefully compare activities of the E- and Z-isomers and the analogs, we determined Ki values against all three forms of mammalian DHFR (Table 3). First, we observed a consistent but not quite statistically significant difference in the Ki values between the E- and Z-isomers, **1a** and **1b**. In all cases the E-isomer was less active than the Z-isomer and the difference ranged from about 2.5-fold to 4-fold. Moreover, an artificially created E/Z-geometric isomer (1:1) mixture showed a Ki value between the values for the two isomers for mDHFR. Among the unsaturated series of analogs, compounds **3**, **4**, and **7** had Ki values against mDHFR close to that of **1b**; for the saturated series the compounds closest to **1b** were **9** and **10**. Therefore in both series, the isopropyl and the cyclopropyl substituents showed the best activity against mDHFR; similar patterns were seen with hDHFR and rIDHFR.

One of the goals of synthesizing the analogs was to increase the hDHFR inhibitory activity of the unsaturated C9-methyl analogs **1a** and **1b**. Compounds **9** and **10** come closest to achieving this goal in that their Ki values are very near that of **1b**. In this series where reduction of the C8–C9 double bond affords conformationally flexible molecules **8–13**, RTK inhibitory activity was observed beyond that for the C9-methyl analogs which were inactive. Compounds **8–11** showed EGFR inhibition and **9** and **10** showed good PDGFR- β inhibition as well. Thus new lead analogs **9** and **10** with dual RTK inhibitory activity against EGFR and PDGFR- β (Table 1) along with acceptable hDHFR activity (Table 2) were discovered.

In summary, the E- and Z-isomers of a previously reported mixture were separated and evaluated as inhibitors of DHFR. In addition, the X-ray crystal structures of these analogs were determined with mDHFR and hDHFR. Twelve 5-substituted furo[2,3-*d*]pyrimidine-2,4-diamines were designed on the basis of the X-ray crystal structures of the lead E- and Z-isomers **1a** and **1b** respectively as multi-targeted RTK inhibitors along with hDHFR inhibition in single molecules to afford combination chemotherapeutic potential in single agents. The biological evaluation identified analogs **3**, **4**, **7**, **9** and **10** as strong inhibitors of mammalian DHFR, in keeping with the structure based design rationale of increasing the length and/or bulk of the alkyl substitution on the C9-position to afford hydrophobic interactions with Val115 in hDHFR. In addition, compounds with comparable or better PDGFR- β inhibitory activity than **1a** and **1b** were also obtained. Conformational restriction of the C8–C9 bond was not an important criteria for DHFR or PDGFR- β inhibitory activity. Both unsaturated and saturated C8–C9 bond analogs were active. Compounds with EGFR inhibitory activity and two (**9** and

10) with dual EGFR and PDGFR- β activity along with good hDHFR activity were discovered. The parent compounds had no EGFR activity. Taken together these results warrant the further development of both the saturated and unsaturated analogs as potential antitumor agents.

Taken together these results suggest that the compounds described in this study can serve as lead analogs for the development of more potent dual RTK and DHFR inhibitors in single molecules.

Experimental Section

Analytical samples were dried in vacuo (0.2 mm Hg) in a CHEM-DRY drying apparatus over P_2O_5 at 80° C. Melting points were determined on a MEL-TEMP II melting point apparatus with FLUKE 51 K/J electronic thermometer and are uncorrected. Nuclear magnetic resonance spectra for proton (1H NMR) were recorded on the Bruker WH-300 (300 MHz) and Bruker Avance II 400 (400 MHz, used for compound **1b** only) spectrometers. The chemical shift values are expressed in ppm (parts per million) relative to tetramethylsilane as an internal standard: s, singlet; d, doublet; t, triplet; q, quartet; m, multiplet; br, broad singlet. The relative integrals of peak areas agreed with those expected for the assigned structures. Thin-layer chromatography (TLC) was performed on POLYGRAM Sil G/UV254 silica gel plates with a fluorescent indicator, and the spots were visualized under 254 and 366 nm illumination. Proportions of solvents used for TLC are by volume. Column chromatography was performed on a 230–400 mesh silica gel (Fisher, Somerville, NJ) column. Elemental analyses were performed by Atlantic Microlab, Inc., Norcross, GA. Element compositions are within 0.4% of the calculated values. Fractional moles of water or organic solvents frequently found in some analytical samples of antifolates could not be prevented in spite of 24–48 h of drying in vacuo and were confirmed where possible by their presence in the 1H NMR spectra. All solvents and chemicals were purchased from Aldrich Chemical Co. or Fisher Scientific and were used as received.

(Z)-5-(2-(2-methoxyphenyl)prop-1-enyl)furo[2,3-d]pyrimidine-2,4-diamine **1b**

To a solution of 5-(chloromethyl)furo[2,3-d]pyrimidine-2,4-diamine (800 mg, 4 mmol) in DMSO (5 mL) was added tributylphosphine (1.2 mL, 6 mmol). After stirring at 60 °C under N_2 for 3 h, the yellowish green solution was cooled to room temperature and sodium hydride (72 mg, 3 mmol) was added followed by 1-(2-methoxyphenyl)ethanone (0.6 mL, 4 mmol). The reaction mixture was stirred at room temperature under N_2 overnight. Two new spots (TLC) with R_f = 0.54 and 0.52 ($CH_3OH:CHCl_3$ = 1:5) appeared and the reaction was quenched with methanol. Purification with a 4 × 25 cm silica gel column was carried out initially with chloroform and then 1% – 2% methanol in chloroform. The fractions at R_f = 0.52 and 0.54 were collected to give the product as a white powder with a yield of 40% (677 mg). The mixture containing both E and Z-isomers was subjected to preparative reverse phase HPLC separation. A Waters® 4000 system with the X-Bridge® C-18 19 × 50 mm column combined with a Waters® 2487 Dual λ Absorbance Detector (245 nm) was used for this purpose. An isocratic scheme was adapted for efficient separation. Details: mobile phase composition, 75% water and 25% acetonitrile; for 0–1 min, 10 ml/min; for 1 min and beyond, 35 ml/min. The sample was prepared with 5 mg of mixture dissolved in 5 mL of methanol and injection was made at 1 mL each time. Retention times for the Z- and E-isomers are 6.580 min and 11.453 min respectively. Purity was confirmed by the same reverse phase HPLC system: mp 237° C – 239° C (decomposed), 1H NMR (DMSO-*d*6): δ 2.09 (s, 3 H, CH_3), 3.70 (s, 3 H, OCH_3), 5.96 (s, 2 H, 4-NH₂, D_2O exchanged), 6.06 (s, 1 H, 6-H), 6.53 (s, 2 H, 2-NH₂, D_2O exchanged), 6.60 (s, 1 H, H double bond), 6.88–6.92 (m, 1 H, C_6H_4), 6.96–6.98 (m, 1 H, C_6H_4), 7.02–7.04 (m, 2 H, C_6H_4), 7.27–7.29 (m, 1 H, C_6H_4). R_f 0.52 ($CH_3OH:CHCl_3$ = 1:5); HRMS *m/z* calcd for $C_{16}H_{17}N_4O_2$ [M+H]⁺, 297.1352; found, 297.1372 [M+H]⁺.

General procedure for the synthesis of compounds 2–7

To a solution of 5-(chloromethyl)furo[2,3-*d*]pyrimidine-2,4-diamine **16**, (0.50 g, 2.5 mmol) in anhydrous DMSO (10 mL) was added tributylphosphine (0.85 g, 3.75 mmol), and the resulting mixture was stirred at 60 °C in an oil bath for 3 h under N₂ to form the phosphonium salt. The deep orange solution was then cooled to room temperature. To this solution was added sodium hydride (95% dispersion in mineral oil, 0.10 g, 3 mmol), followed by the corresponding aryl ketones (2.75 mmol). The reaction mixture was stirred at room temperature for 24–32 h. TLC showed the disappearance of **16** and the formation of two products (TLC). The reaction was quenched with 20 mL methanol, washed with two portions of 50 mL methanol, and the resulting solution was evaporated under reduced pressure to dryness. To the residue was added 3 g of silica gel and CHCl₃ (20 mL) and the slurry was loaded onto a 4 × 20 cm dry silica gel column and flash chromatographed initially with CHCl₃ (300 mL), then sequentially with 2% MeOH in CHCl₃ (250 mL), 5% MeOH in CHCl₃ (300 mL), and 8% MeOH in CHCl₃ (250 mL). Fractions which showed the desired spot on TLC were pooled and evaporated to dryness and the residue was recrystallized from ethylacetate to afford the desired olefinic targets **2–7**.

5-[(Z/E)-2-(2'-methoxyphenyl)pent-1-en-1-yl]furo[2,3-*d*]pyrimidine-2,4-diamine (2)

Using the general method above compound **16** (0.50 g, 2.5 mmol) and 1-(2-methoxyphenyl)butan-1-one (0.49 g, 2.75 mmol) afforded **2** (0.20 g, 25%) as white crystals: mp 222–224 °C; *R*_f = 0.57 and 0.58 (MeOH/CHCl₃, 1:5); ¹H NMR (DMSO-*d*₆) (*E/Z* 2:1) *E*-isomer δ 0.70 (t, 3 H, *J* = 7.6 Hz), 1.14–1.21 (m, 4 H), 3.79 (s, 3 H), 6.09 (s, 2 H), 6.33 (s, 1 H), 6.87 (s, 2 H), 6.96–7.29 (m, 4 H), 7.41 (s, 1 H); *Z*-isomer δ 0.72 (t, 3 H, *J* = 7.6 Hz), 1.16–1.21 (m, 4 H), 3.86 (s, 3 H), 6.09 (s, 2 H), 6.13 (s, 1 H), 6.42 (s, 2 H), 6.65 (s, 1 H), 6.93–7.26 (m, 4 H). Anal. (C₁₈H₂₀N₄O₂) C, H, N.

5-[(Z/E)-2-(2'-methoxyphenyl)-3-methylbut-1-en-1-yl]furo[2,3-*d*]pyrimidine-2,4-diamine (3)

Using the general method above compound **16** (0.50 g, 2.5 mmol) and 1-(2-methoxyphenyl)-2-methylpropan-1-one (0.49 g, 2.75 mmol) afforded **3** (0.16 g, 20%) as white crystals: mp 217–219 °C; TLC *R*_f = 0.55 and 0.56 (MeOH/CHCl₃, 1:5); ¹H NMR (DMSO-*d*₆) (*E/Z* 3:1) *E*-isomer δ 1.05 (m, 6 H), 2.73–2.89 (m, 1 H), 3.68 (s, 3 H), 5.96 (s, 2 H), 6.41 (s, 2 H), 6.53 (s, 1 H), 6.88–7.27 (m, 4 H), 7.32 (s, 1 H); *Z*-isomer 1.23 (m, 6 H), 2.75–2.98 (m, 1 H), 3.78 (s, 3 H), 5.99 (s, 2 H), 6.10 (s, 1 H), 6.45 (s, 2 H), 6.53 (s, 1 H), 6.90–7.23 (m, 4 H). Anal. (C₁₈H₂₀N₄O₂) C, H, N. HRMS (EI) calcd for C₁₈H₂₀N₄O₂ 324.1587, found 324.1586.

5-[(Z/E)-2-Cyclopropyl-2-(2'-methoxyphenyl)vinyl]furo[2,3-*d*]pyrimidine-2,4-diamine (4)

Using the general method above compound **16** (0.50 g, 2.5 mmol) and cyclopropyl(2-methoxyphenyl)methanone (0.48 g, 2.7 mmol) afforded **4** (0.12 g, 15%) as white crystals: mp 198–199 °C; TLC *R*_f = 0.57 and 0.58 (CH₃OH/CHCl₃, 1:5); ¹H NMR (DMSO-*d*₆) (*E/Z* 2:1) *E* isomer δ 0.60–0.63 (m, 4 H), 1.84–1.96 (m, 1 H), 3.84 (s, 3 H), 5.96 (s, 2 H), 6.45 (s, 2 H), 6.53 (s, 1 H), 6.88–7.32 (m, 4 H), 7.45 (s, 1 H). *Z*-isomer 0.63–0.66 (m, 4 H), 1.96–1.97 (m, 1 H), 6.06 (s, 2 H), 6.50 (s, 1 H), 6.77 (s, 2 H), 6.94 (s, 1 H), 7.01–7.34 (m, 4 H). Anal. (C₁₈H₁₈N₄O₂) C, H, N.

5-[(Z/E)-2-(2'-methoxyphenyl)hex-1-en-1-yl]furo[2,3-*d*]pyrimidine-2,4-diamine (5)

Using the general method above compound **16** (0.50 g, 2.5 mmol) and 1-(2-methoxyphenyl)pentan-1-one (0.52 g, 2.7 mmol) afforded **5** (0.14 g, 17%) as white crystals: mp 195–198 °C; *R*_f = 0.57 and 0.58 (MeOH/CHCl₃, 1:5); ¹H NMR (DMSO-*d*₆) (*E/Z* 3:2) *E*-isomer δ 0.70 (m, 3 H), 0.85 (m, 2 H), 1.14 (m, 2 H), 1.29 (m, 2 H), 3.80 (s, 3 H), 5.96 (s, 2 H), 6.41 (s, 2 H), 6.59 (s, 1 H), 6.93–7.27 (m, 4 H), 7.30 (s, 1 H). *Z*-isomer 0.70 (m, 3 H), 0.85 (m, 2 H), 1.14 (m, 2 H), 1.29 (m, 2 H), 3.70 (s, 3 H), 6.32 (s, 1 H), 6.59 (s, 1 H), 6.96–7.21 (m, 4 H). Anal. (C₁₉H₂₂N₄O₂ · 0.25H₂O) C, H, N.

5-[*(Z/E*)-2-(2'-methoxyphenyl)-4-methylpent-1-en-1-yl]furo[2,3-*d*]pyrimidine-2,4-diamine (6**)**

Using the general method above compound **16** (0.50 g, 2.5 mmol) and 1-(2-methoxyphenyl)-3-methylbutan-1-one (0.50 g, 2.7 mmol) afforded **6** (0.20 g, 24%) as white crystals: mp 221–223 °C; R_f = 0.59 and 0.61 (MeOH/CHCl₃, 1: 5); ¹H NMR (DMSO-*d*₆) (*E/Z* 2:1) *E*-isomer δ 0.72–0.72 (d, 6 H, *J* = 6.4 Hz), 1.34–1.57 (m, 1 H), 2.34–2.36 (m, 4 H), 3.81 (s, 3 H), 5.95 (s, 2 H), 6.08 (s, 2 H), 6.36 (s, 1 H), 6.93–7.27 (m, 4 H), 7.27 (s, 1 H); *Z*-isomer 0.87 (d, 6 H, *J* = 6.2 Hz), 1.48–1.57 (m, 1 H), 2.36–2.44 (m, 4 H), 6.11 (s, 2 H), 6.41 (s, 2 H), 6.46 (s, 1 H), 6.58 (s, 1 H), 6.94–7.25 (m, 4 H). Anal. (C₁₉H₂₂N₄O₂ · 0.9H₂O) C, H, N.

5-[*(Z/E*)-2-(2'-methoxyphenyl)-3-methylpent-1-en-1-yl]furo[2,3-*d*]pyrimidine-2,4-diamine (7**)**

Using the general method above compound **16** (0.50 g, 2.5 mmol) and 1-(2-methoxyphenyl)-2-methylbutan-1-one (0.50 g, 2.7 mmol) affords **7** (0.18 g, 22%) as white crystals: mp 202–204 °C; R_f = 0.62 and 0.64 (MeOH/CHCl₃, 1: 5); ¹H NMR (DMSO-*d*₆) (*E/Z* 3:2) δ *E*-isomer 0.77–0.82 (t, 3 H, *J* = 7.6 Hz), 0.87–0.91 (m, 3 H), 0.93–1.53 (m, 2 H), 2.63 (m, 1 H), 3.67 (s, 3 H), 5.95 (s, 2 H), 6.43 (s, 2 H), 6.52 (s, 1 H), 6.89–7.28 (m, 4 H), 7.30 (s, 1 H); *Z*-isomer 0.77–0.82 (t, 3 H, *J* = 7.6 Hz), 0.89–0.93 (m, 3 H), 0.93–1.51 (m, 2 H), 2.53 (m, 1 H), 3.78 (s, 3 H), 5.95 (s, 2 H), 6.09 (s, 1 H), 6.52 (s, 2 H), 6.92 (s, 1 H), 6.89–7.28 (m, 4 H). Anal. (C₁₉H₂₂N₄O₂ · 0.3H₂O) C, H, N.

General procedure for the synthesis of 8–13

To a solution of the olefinic intermediate (0.3–0.5 mmol) in a mixture of CHCl₃ (50 mL) and MeOH (15 mL) was added 5% palladium on activated carbon (0.2 g), and the suspension was hydrogenated in a Parr apparatus at 50–55 psi for 12–24 h. TLC indicated the disappearance of the starting material and the formation of one major spot. The reaction mixture was filtered through Celite, washed with 30% MeOH in CHCl₃ 50 mL. After evaporation of the solvent, MeOH 50 mL was added to afford a solution. To this solution was added 5 g silica gel and the mixture was evaporated under reduced pressure to dryness. This silica gel plug was loaded on a dry silica gel column and flash chromatographed initially with CHCl₃ 150 mL, then sequentially with 1% MeOH in CHCl₃ (150 mL), 2% MeOH in CHCl₃ (150 mL), and 5% MeOH in CHCl₃ (150 mL). Fractions which showed the major spot on TLC were pooled and evaporated to dryness. The residue was recrystallized from MeOH, or other solvent combinations as indicated, to afford the desired target compounds **8–13**.

5-[*(R/S*)-2-(2'-methoxyphenyl)pentyl]furo[2,3-*d*]pyrimidine-2,4-diamine (8**)**

Using the general method above compound **2** (152 mg, 0.46 mmol) at 50 psi for 22 h afforded **8** (100 mg, 45%) as white crystals: mp 210–212 °C; R_f = 0.54 (MeOH/CHCl₃, 1:9); ¹H NMR (DMSO-*d*₆) δ 0.75–0.79 (t, 3 H, *J* = 6.9 Hz), 1.04–1.23 (m, 2 H), 1.59–1.61 (m, 2 H), 2.68–2.78 (m, 2 H), 3.29 (m, 1 H), 3.76 (s, 3 H), 4.03–4.22 (m, 1 H), 5.65–5.77 (s, 2 H), 5.98 (s, 2 H), 6.91 (s, 1 H), 6.94–7.22 (m, 4 H). HRMS (EI) calcd for C₁₈H₂₂N₄O₂ 327.1821, found 327.1775.

5-[*(R/S*)-2-(2-methoxyphenyl)-3-methylbutyl]furo[2,3-*d*]pyrimidine-2,4-diamine (9**)**

Using the general method above compound **3** (115 mg, 0.35 mmol) at 55 psi for 22 h. Following chromatography the fractions containing the product were pooled and evaporated and the residue recrystallized from MeOH/CH₃COCH₃ to afford **9** (100 mg, 65%) as white crystals: mp 210–212 °C; R_f = 0.53 (MeOH/CHCl₃, 1:9); ¹H NMR (DMSO-*d*₆) δ 0.95 (d, 6 H, *J* = 6.9 Hz), 1.15 (m, 1 H), 1.35–2.18 (m, 2 H), 2.81 (m, 1 H), 3.75 (s, 3 H), 4.03–4.22 (m, 1 H), 5.65 (s, 2 H), 5.98 (s, 2 H), 6.13 (s, 1 H), 6.63–7.31 (m, 4 H). Anal. (C₁₈H₂₂N₄O₂ · 0.25 CH₃COCH₃) C, H, N.

5-[(R/S)-2-cyclopropyl-2-(2'-methoxyphenyl)ethyl]furo[2,3-d]pyrimidine-2,4-diamine (10)—Using the general method above compound **4** (118 mg, 0.36 mmol) at 55 psi for 24 h afforded **10** (40 mg, 34%) as white crystals: mp 178–179 °C; R_f = 0.57–0.58 (MeOH/CHCl₃, 1:9); ¹H NMR (DMSO-*d*₆) δ 0.16 (m, 4 H), 0.62 (m, 1 H), 2.92 (m, 2 H), 3.01 (m, 1 H), 3.78 (s, 3 H), 4.00–4.11 (m, 1 H), 5.97 (s, 2 H), 6.37 (s, 2 H), 6.95 (s, 1 H), 6.96–6.98 (m, 4 H). Anal. (C₁₈H₂₀N₄O₂) C, H, N. HRMS (EI) calcd for C₁₈H₂₀N₄O₂ 324.1586, found 324.1577.

5-[(R/S)-2-(2'-methoxyphenyl)hexyl]furo[2,3-d]pyrimidine-2,4-diamine (11)—Using the general method above compound **5** (125 mg, 0.36 mmol) at 50 psi for 19 h afforded **11** (44 mg, 36%) as white crystals: mp 184–186 °C; R_f = 0.47 (MeOH/CHCl₃, 1:9); ¹H NMR (DMSO-*d*₆) δ 0.70–0.74 (t, 3 H, *J* = 3.6 Hz), 0.76–1.04 (m, 2 H), 1.19–1.63 (m, 2 H), 1.75–2.05 (m, 2 H), 2.71 (m, 1 H), 3.59 (m, 2 H), 3.83 (s, 3 H), 5.96 (s, 2 H), 6.32 (s, 2 H), 6.58 (s, 1 H), 6.91–7.29 (m, 4 H). Anal. (C₁₉H₂₄N₄O₂) C, H, N.

5-[(R/S)-2-(2'-methoxyphenyl)-4-methylpentyl]furo[2,3-d]pyrimidine-2,4-diamine (12)—Using the general method above compound **6** (334 mg, 0.98 mmol) at 50 psi for 24 h afforded **12** (103 mg, 31%) as white crystals: mp 192–194 °C; R_f = 0.57 (MeOH/CHCl₃, 1:9); ¹H NMR (DMSO-*d*₆) δ 0.77–0.79 (d, 6 H), 1.22–1.66 (m, 1 H), 1.90–2.05 (m, 2 H), 2.50–2.79 (m, 2 H), 3.77 (s, 3 H), 4.01–4.24 (m, 1 H), 5.65 (s, 2 H), 5.02 (s, 2 H), 6.56 (s, 1 H), 6.93–7.29 (m, 4 H). Anal. (C₁₉H₂₄N₄O₂) C, H, N.

5-[(R/S)-2-(2'-methoxyphenyl)-3-methylpentyl]furo[2,3-d]pyrimidine-2,4-diamine (13)—Using the general method above compound **7** (140 mg, 0.4 mmol) at 50 psi for 24 h afforded **13** (85 mg, 60%) as white crystals: mp 185–187 °C; R_f = 0.52 (CH₃OH/CHCl₃, 1:9); ¹H NMR (DMSO-*d*₆) δ 0.62–0.75 (m, 3 H), 0.83–0.91 (m, 3 H), 1.04–1.17 (m, 2 H), 1.19–2.20 (m, 1 H), 2.70 (m, 1 H), 3.06 (m, 2 H), 3.73 (s, 3 H), 5.92 (s, 2 H), 6.34 (s, 2 H), 6.60 (s, 1 H), 6.94–7.36 (m, 4 H). Anal. (C₁₉H₂₄N₄O₂) C, H, N.

Crystallization and X-ray Data Collection

Recombinant mouse DHFR was expressed and purified as described previously,⁴⁴ as was the human DHFR enzyme.³¹ The mDHFR protein was washed in a centricon-10 with 10 mM HEPES buffer, pH 7.4 and concentrated to 33.2 mg/mL. The protein was incubated with NADPH and a 10:1 molar excess of the inhibitor, **1a** or **1b**, for one hour over ice prior to crystallization using the hanging drop vapor diffusion method. Protein droplets contained 170–200 mM Tris, pH 8.3, 85 mM Na cacodylate, 25% PEG 4K, 15% glycerol. Crystals grew over several weeks time and are monoclinic, space group P21 and diffracted to 2.1 Å and 1.4 Å resolution for the E- and Z-isomer, respectively. Data were collected at liquid N₂ temperatures on a Rigaku RaxisIV imaging plate system with MaxFlux optics and the data processed with using both Denzo⁴⁵ and Mosflm.⁴⁶ Diffraction statistics are shown in Table 4 for both complexes.

The human DHFR protein was washed in a Centricon-10 three times with 50 mM phosphate buffer, pH 6.9 in 100 mM KCl buffer and concentrated to 5.3 mg/ml and incubated overnight at 4°C with a molar excess of NADPH followed by the inhibitor **1a**. Protein droplets contained variable amounts of ammonium sulfate (60–70%) at pH 6.9. and 3% ethanol. Crystals were grown using hanging drop vapor diffusion on glass cover slips using experiments were carried out at 14°C. Data were collected at the Stanford Synchrotron Resource Laboratory on beamline 9-2. Diffraction statistics for the current refinement are shown in Table 4.

The mDHFR structures were solved by molecular replacement methods using the coordinates for mouse DHFR (2FZJ) in the program Molref.⁴⁶ Similarly, the hDHFR structure was solved

by molecular replacement methods using the coordinates for hDHFR (1U72). Inspection of the resulting difference electron density maps were made using the program COOT⁴⁷ running on a Mac G5 workstation and revealed density for a ternary complex with mDHFR (Figure 3 and Figure 4). To monitor the refinement, a random subset of all reflections was set aside for the calculation of Rfree (5%). The model for the inhibitors E-isomer **1a** and Z-isomer **1b** were modeled on those using the builder function in Sybyl³⁴ and the parameter file for the inhibitors were prepared using the Dundee PRODGR2 Server website (<http://davapc1.bioch.dundee.ac.uk/programs/prodrg>). The final cycles of refinement were carried out using the program Refmac5 in the CCP4 suite of programs.⁴⁶ The Ramachandran conformational parameters from the last cycle of refinement generated by PROCHECK⁴⁸ showed that more than 89.9% of the residues in both E-isomer and Z-isomer mDHFR complexes have the most favored conformation and none are in the disallowed regions. Coordinates for the mDHFR complexes have been deposited with the Protein Data Bank (PDB code 3d7y and 3d7x). Coordinates for the hDHFR complex will be deposited after further refinement.

Dihydrofolate Reductase Evaluations

Kinetic Properties

Kinetic properties of the recombinant mouse DHFR were determined and compared to those of recombinant human DHFR and native rat liver DHFR (Table 5). The kinetic properties of the recombinant mouse DHFR used in these studies are comparable to those published previously by others. Values for k_{cat} were reported by Dicker et al.⁴⁹ to be 2.2 s-1 (measured at 25° C) and by Thillet et al.⁵⁰ as 7 s-1 (measured at 30° C); our value of 29s-1 compares well, considering that the current measurements were made at 37° C. Values for the K_m for NADPH of 14 μM (20) and 0.54 μM (19) do not agree particularly well with each other but the value reported herein (2.4 μM) lies between the two reported values. The value of 0.32 μM we report of the K_m for DHFA agrees well with the value of 0.36 μM reported by Dicker et al.⁴⁹

Standard DHFR assays were conducted at 37° C with continuous recording of change of OD at 340 nM. The assay contained 41 nM sodium phosphate buffer at pH 7.4, 2-mercaptoethanol 8.9 mM, 150 mM KCl, and saturating concentrations of NADPH and dihydrofolic acid (DHFA). With mouse DHFR, the standard DHFA concentration was 18 μM, but for the human enzyme standard conditions included 90 μM DFHA; 117 μM NADPH was used for both DHFR forms. Initial rates of enzyme activity were measured; rates were linear under standard conditions for about 2 min. for mDHFR and for over 5 min. for hDHFR. Activity was linearly related to protein concentration under these conditions of assay.

K_m values were determined by holding either substrate or cofactor at a constant, saturating concentration and varying the other over a range of concentrations. The K_m value was determined by fitting the data to the Michaelis-Menton equation using nonlinear regression methods (Prism 4.0). The value of k_{cat} was determined from the Vmax value and the protein concentration ($k_{cat} = V_{max}[E_{tot}]$).

K_i values were determined by measuring inhibition of the reaction at two or more concentrations of substrate (DHFA). For the competitive inhibitors in this study, K_i could be calculated from the equation:

$$K_i = IC_{50}/(1 + S/K_m)$$

All determinations of IC₅₀ were made by fitting percent inhibition data to a single site sigmoidal model with variable slope, using nonlinear regression methods (Prism 4.0). All inhibition curves required at least four points within the central segment of the sigmoidal curve. Statistical comparisons were preformed with InStat 2.03, using the nonparametric Welch t test because variances among groups could not be shown to be equal; this test is more conservative than the standard test.

Receptor Tyrosine Kinase Evaluations

Cells

All cells were maintained at 37° C in a humidified environment containing 5% CO₂ using media from Mediatech (Hemden, NJ). A-431 cells were from the American Type Tissue Collection (Manassas, VA).

Chemicals

All growth factors (bFGF, VEGF, EGF, PDGF-BB) were purchased from Peprotech (Rocky Hill, NJ). PD153035, SU5416, AG1295 and VEGF kinase inhibitor (4-[4'-Chloro-2'-fluoro]phenylamino]-6,7-dimethoxyquinazoline) were purchased from Calbiochem (San Diego, CA). The CYQUANT cells proliferation assay was from Molecular Probes (Eugene, OR). All other chemicals were from Sigma Chemical unless otherwise noted.

Antibodies

The PY-HRP antibody was from BD Transduction Laboratories (Franklin Lakes, NJ). Antibodies against EGFR, PDGFR β , FGFR-1, Flk-1, and Flt-1 were purchased from Upstate Biotech (Framingham, MA).

Phosphotyrosine Cytoblot

Cells used were tumor cell lines naturally expressing high levels of EGFR (A431), Flk-1 (U251), Flt-1 (A498), and PDGFR- β (SF-539). Expression levels at the RNA level were derived from the NCI Developmental Therapeutics Program (NCI-DTP) web site public molecular target information (http://www.dtp.nci.nih.gov/mttargets/mt_index.html). Briefly, cells at 60–75% confluence are placed in serum-free medium for 18 h to reduce the background of phosphorylation. Cells were always >98% viable by Trypan blue exclusion. Cells are then pretreated for 60 min with 10, 3.33, 1.11, 0.37, and 0.12 μ M compound followed by 100 ng/ml EGF, VEGF, PDGF-BB, or bFGF for 10 min. The reaction is stopped and cells permeabilized by quickly removing the media from the cells and adding ice-cold Tris-buffered saline (TBS) containing 0.05% Triton X-100, protease inhibitor cocktail and tyrosine phosphatase inhibitor cocktail. The TBS solution is then removed and cells fixed to the plate for 30 min at 60 °C and further incubation in 70% ethanol for an additional 30 min. Cells are further exposed to block (TBS with 1% BSA) for 1 h, washed, and then a horseradish peroxidase (HRP)-conjugated phosphotyrosine (PY) antibody added overnight. The antibody is removed, cells are washed again in TBS, exposed to an enhanced luminal ELISA substrate (Pierce Chemical, Rockford, IL) and light emission measured using a plate reader (BMG Labtech, Durham, NC). The known RTK-specific kinase inhibitor PD153035 was used as a positive control compound for EGFR kinase inhibition; SU5416 for Flk1 kinase inhibition; AG1295 for PDGFR- β kinase inhibition; and CB676475 (4-[(4'-chloro-2'-fluoro)phenylamino]-6,7-dimethoxyquinazoline) was used as a positive control for both Flt1 and Flk1 kinase inhibition. Data were graphed as a percent of cells receiving growth factor alone and IC₅₀ values were calculated from two to three separate experiments (n = 8–17) using Prism 5.0 (GraphPad Software, San Diego CA).

CYQUANT cell proliferation assay

As a measure of cell proliferation, the CYQUANT cell counting/proliferation assay was used as previously described.⁵¹ Briefly, cells are first treated with compounds for 12 hr and allowed to grow for an additional 36 hr. The cells are then lysed and the CYQUANT dye, which intercalates into the DNA of cells, is added and after 5 min the fluorescence of each well measured using an UV Products BioChemi digital darkroom. A Positive control used for cytotoxicity in each experiment was cisplatin, with an apparent average IC₅₀ value of 8.2±0.65 μM. Data are graphed as a percent of cells receiving growth factor alone and IC₅₀ values estimated from 2–3 separate experiments (n = 6–15) using Probit plots.

Chorioallantoic membrane (CAM) assay of angiogenesis

The CAM assay is a standard assay for testing antiangiogenic agents.⁵² The CAM assay used in these studies was modified from a procedure by Sheu⁵³ and Brooks⁵⁴ and as published previously.⁵⁵ Briefly, fertile leghorn chicken eggs (CBT Farms, Chestertown, MD) are allowed to grow until 10 days of incubation. The proangiogenic factors human VEGF-165 and bFGF (100 ng each) are then added to saturation to a 6 mm microbial testing disc (BBL, Cockeysville, MD) and placed onto the CAM by breaking a small hole in the superior surface of the egg. Antiangiogenic compounds are added 8 hr after the VEGF/bFGF at saturation to the same microbial testing disk and embryos allowed to incubate for an additional 40 hr. After 48 hr, the CAMs are perfused with 2% paraformaldehyde/3% glutaraldehyde containing 0.025% Triton X-100 for 20 seconds, excised around the area of treatment, fixed again in 2% paraformaldehyde/3% glutaraldehyde for 30 min, placed onto Petri dishes, and a digitized image taken using a dissecting microscope (Wild M400; Bannockburn, IL) at 7.5x and SPOT Enhanced digital imaging system (Diagnostic Instruments, Sterling Heights, MI). A grid is then added to the digital CAM images and the average number of vessels within 5–7 grids counted as a measure of vascularity. AGM-1470 (a kind gift of the NIH Developmental Therapeutics Program) and SU5416 are used as a positive control for antiangiogenic activity. Data are graphed as a percent of CAMs receiving bFGF/VEGF and IC₅₀ values estimated from 2–3 separate experiments (n=5–11) using Probit plots.

Supplementary Material

Refer to Web version on PubMed Central for supplementary material.

Abbreviations

RTK, receptor tyrosine kinase; VEGFR, vascular endothelial growth factor receptor; EGFR, epidermal growth factor receptor; PDGFR, platelet-derived growth factor receptor; FGFR, fibroblast growth factor receptor; ATP, Adenosine 5'-triphosphate; DHFR, dihydrofolate reductase; MTX, methotrexate.

Acknowledgments

This work was supported, in part, by the National Institutes of Health Grants, National Cancer Institute CA09885 (A.G.), National Institute of Allergy and Infectious Diseases AI069966 (A.G.) and the National Institute of General Medical Sciences GM51670 (VC). VC acknowledges Jennifer Makin, Jennifer Piraino and Jessica Nowak for their efforts on the cloning, expression and crystallization of the human DHFR complex. The National Science Foundation, CHE 0614785, is acknowledged for NMR facilities.

References

1. Folkman J. New Eng. J. Med 1971;285:1182. [PubMed: 4938153]

2. Fox, SB.; Harris, AL. New Angiotherapy. Fan, TP.; Kohn, EC., editors. Totowa, NJ: Humana Press; 2002. p. 151-176.
3. Cherrington JM, Strawn LM, Shawver LK. *Adv. Can. Res* 2000;20:1.
4. Sun L, McMahon G. *Drug Discov. Today* 2000;5:344. [PubMed: 10893547]
5. Shauver, LK.; Lipson, KE.; Fong, TAT.; McMahon, G.; Strawn, LM. The New Angiotherapy. Fan, TP.; Kohn, EC., editors. Totowa, NJ: Humana Press; 2002. p. 409-452.and references therein
6. Hubbard SR, Till JH. *Annu. Rev. Biochem* 2000;69:373. [PubMed: 10966463]
7. Shin DM, Ro JY, Hong WK, Hittelmann WN. *Cancer Res* 1994;54:3153. [PubMed: 8205534]
8. Tateishi M, Ishida T, Mitsudomi T, Kaneko S, Sugimachi K. *Cancer Res* 1990;50:7077. [PubMed: 2208175]
9. Gorgoulis V, Aninos D, Mikou P, Kanavaros P, Karameris A, Joardanoglu J, Rasidakis A, Veslemes M, Ozanne B, Spandidos DA. *Anticancer. Res* 1992;12:1183. [PubMed: 1503407]
10. Fleming TP, Saxena A, Clark WC, Robertson JT, Oldfield EH, Aaronson SA, Ali IU. *Cancer Res* 1992;52:4550. [PubMed: 1322795]
11. Maxwell M, Naber SP, Wolfe HJ, Galanopoulos T, Hedley-Whyte ET, Black PM, Antoniades HN. *J. Clin. Invest* 1990;86:131. [PubMed: 2164040]
12. Hermanson M, Funa K, Hartman H, Claesson-Welsh L, Heldin CH. *Cancer Res* 1992;52:3213. [PubMed: 1317261]
13. Ross JS, Fletcher JA. *Stem Cells* 1998;16:413. [PubMed: 9831867]
14. Benjamin LE, Keshet E. *Proc. Natl. Acad. Sci. USA* 1997;94:8761. [PubMed: 9238051]
15. Benjamin LE, Golijanin D, Itin A, Pode D, Keshet E. *J. Clin. Invest* 1999;103:159. [PubMed: 9916127]
16. Burns C, Liu W, Shaheen R, Davis D, McConkey D, Wilson M, Bucana C, Hicklin D, Ellis L. *Cancer (Phila.)* 2000;89:488. [PubMed: 10931447]
17. Carmeliet P, Dor Y, Herbert JM, Fukumura D, Brusselmans K, Dewerchin M, Neeman M, Bono F, Abramovitch R, Maxwell P, Koch CJ, Ratcliffe P, Moons L, Jain RK, Collen D, Keshet E. *Nature (Lond.)* 1998;394:485. [PubMed: 9697772]
18. Pearson, M.; Garcia-Echeverria, C.; Fabbro, D. Protein Tyrosine Kinases. From Inhibitors to Useful Drugs. Fabbro, D.; McCormick, F., editors. Totowa, NJ: Humana Press; 2006. p. 1-29.
19. Quesada AR, Muñoz-Chápuli R, Medina MA. *Med. Res. Rev* 2006;26:483. [PubMed: 16652370]
20. Zhang J, Yang PL, Gray NS. *Nature Rev. Cancer* 2009;9:28. [PubMed: 19104514]
21. Cohen RB. *Clin. Colorectal Cancer* 2003;2:246. [PubMed: 12620146]
22. Wedge, SR.; Jürgensmeier, JM. Tumor Angiogenesis. Basic Mechanisms and Cancer Therapy. Marmé, D.; Fusenig, N., editors. Germany: Springer-Verlag, Berlin Heidelberg; 2008. p. 395-423.
23. Östman, A.; Betsholtz, C. Tumor Angiogenesis. Basic Mechanisms and Cancer Therapy. Marmé, D.; Fusenig, N., editors. Germany: Springer-Verlag, Berlin Heidelberg; 2008. p. 155-169.
24. Rosowsky A. *Prog. Med. Chem* 1989;26:1. [PubMed: 2690183]
25. Gangjee A, Jain HD, Kurup S. *Anti-Cancer Agents in Med. Chem* 2007;7:524.
26. Gangjee A, Jain HD, Kurup S. *Anti-Cancer Agents in Med. Chem* 2008;8:205.
27. Cody V, Luft JR, Pangborn W, Gangjee A. *Acta Cryst. D. Biol. Crystallogr* 2003;59:1603. [PubMed: 12925791]
28. Gangjee A, Zeng Y, Ihnat M, Warnke LA, Green DW, Kisliuk RL, Lin F-T. *Bioorg. Med. Chem* 2005;13:5475. [PubMed: 16039863]
29. Cody V, Pace J, Chisum K. *Proteins, Structure, Function and Bioinformatics* 2006;65:959.
30. Cody V, Luft JR, Pangborn W. *Acta Cryst* 2005;D61:147.
31. Cody V, Galitsky N, Luft JR, Pangborn W, Gangjee A, Devraj R, Queener SF, Blakely RL. *Acta Cryst* 1997;D53:638.
32. Cody V, Galitsky N, Rak D, Luft JR, Pangborn W, Queener SF. *Biochemistry* 1999;38:4303. [PubMed: 10194348]
33. DeLano Scientific LLC., PyMol.
34. Tripos Inc., 1699 South Hanley Road, St. Louis, MO 63144.

35. Gangjee A, Yu J, Kisliuk RL, Haile WH, Sobrero G, McGuire JJ. *J. Med. Chem.* 2003;46:59.
36. Henry G, John E. *J. Am. Chem. Soc.* 1957;79:2150.
37. Corey EJ, Suggs JW. *Tetrahedron Letters* 1975;31:2647.
38. Liang X, Bols M. *J. Chem. Soc., Perkin Trans* 2002;1:503.
39. Gangjee A, Zeng Y, McGuire JJ, Kisliuk RL. *J. Med. Chem.* 2000;43:3125. [PubMed: 10956221]
40. Stockwell BR, Haggarty SJ, Schreiber SL. *Chem. Biol.* 1999;6:71. [PubMed: 10021420]
41. Schilder RJLH, Monks A, Handel LM, Fornace AJ, Ozols RF, Fojo AT, Hamilton TC. *Int. J. Cancer* 1990;45:416. [PubMed: 2307530]
42. Vu MT, Smith CF, Burger PC, Klintworth GK. *Lab. Invest.* 1985;53:499. [PubMed: 2413278]
43. Gangjee A, Yang J, Ihnat MA, Kamat S. *Bioorg. Med. Chem.* 2003;11:5155. [PubMed: 14604679]
44. Cody V, Pace J, Rosowsky A. *Acta Cryst* 2008;D64:977.
45. Otwinowski, Z.; Minor, W. *Methods in Enzymology*. Carter, CW., Jr; Sweet, RM., editors. Vol. Vol 276. New York: Academic Press; 1997. p. 224-225.
46. Collaborative Computational Project, Number 4, The CCP4 Suite: Programs for Protein Crystallography. *Acta Crystallogr* 1994;D50:760–763.
47. Emsley P, Cowtan K. *Acta Crystallogr* 2004;D60:2126.
48. Laskowski RA, MacArthur MW, Moss DS, Thornton JM. *J. Applied Crystallogr* 1993;26:283.
49. Dicker AP, Waltham MC, Volkenandt M, Schweitzer BI, Otter GM, Schmid FA, Sirotnak FM, Bertino JR. *Proc. Natl. Acad. Sci. USA* 1993;90:11797. [PubMed: 8265628]
50. Thillet J, Absil J, Stone SR, Pictet R. *J. Biol. Chem.* 1988;263:12500. [PubMed: 3045118]
51. Wilson SM, Barsoum MJ, Wilson BW, Pappone PA. *Cell Prolif* 1999;32:131. [PubMed: 10535359]
52. Vu MT, Smith CF, Burger PC, Klintworth GK. *Lab. Invest.* 1985;53:499. [PubMed: 2413278]
53. Sheu JR, Fu CC, Tsai ML, Chung WJ. *Anticancer Res* 1998;18:4435. [PubMed: 9891506]
54. Brooks PC, Montgomery AM, Cheresh DA. *Methods Mol. Biol.* 1999;129:257. [PubMed: 10494570]
55. Marks MG, Shi J, Fry MS, Xiao Z, Trzyna M, Pokala V, Ihnat MA, Li P-K. *Biol. Pharm. Bull.* 2002;25:597. [PubMed: 12033499]

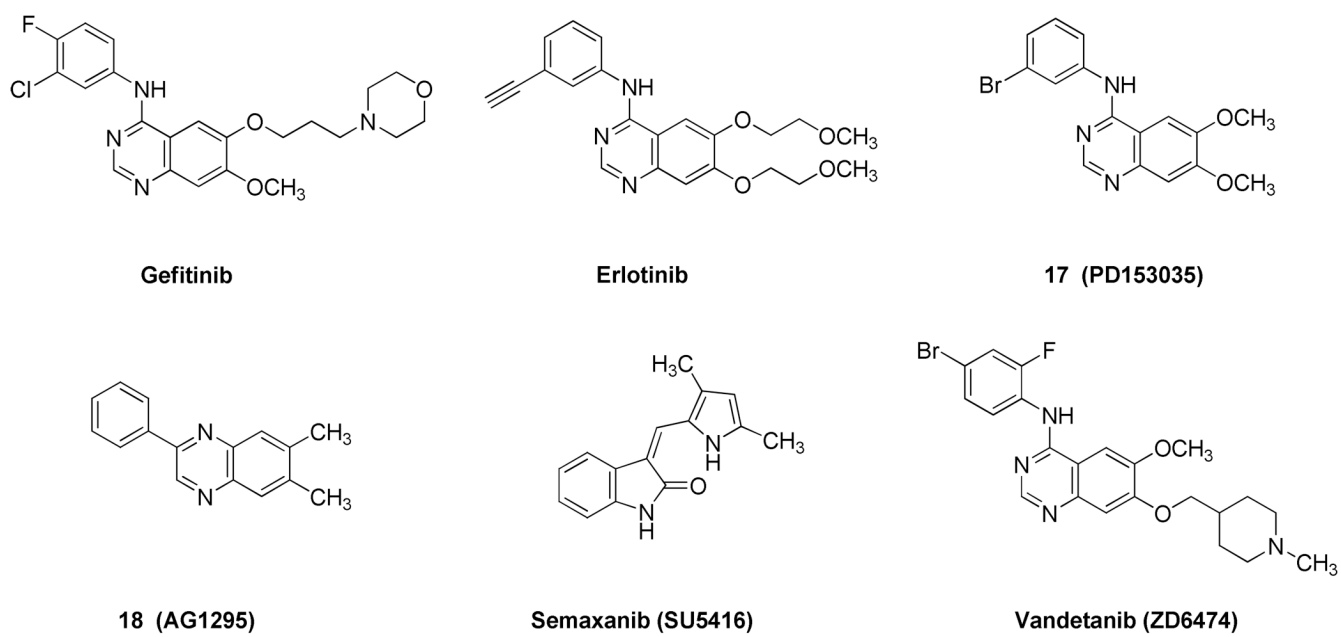
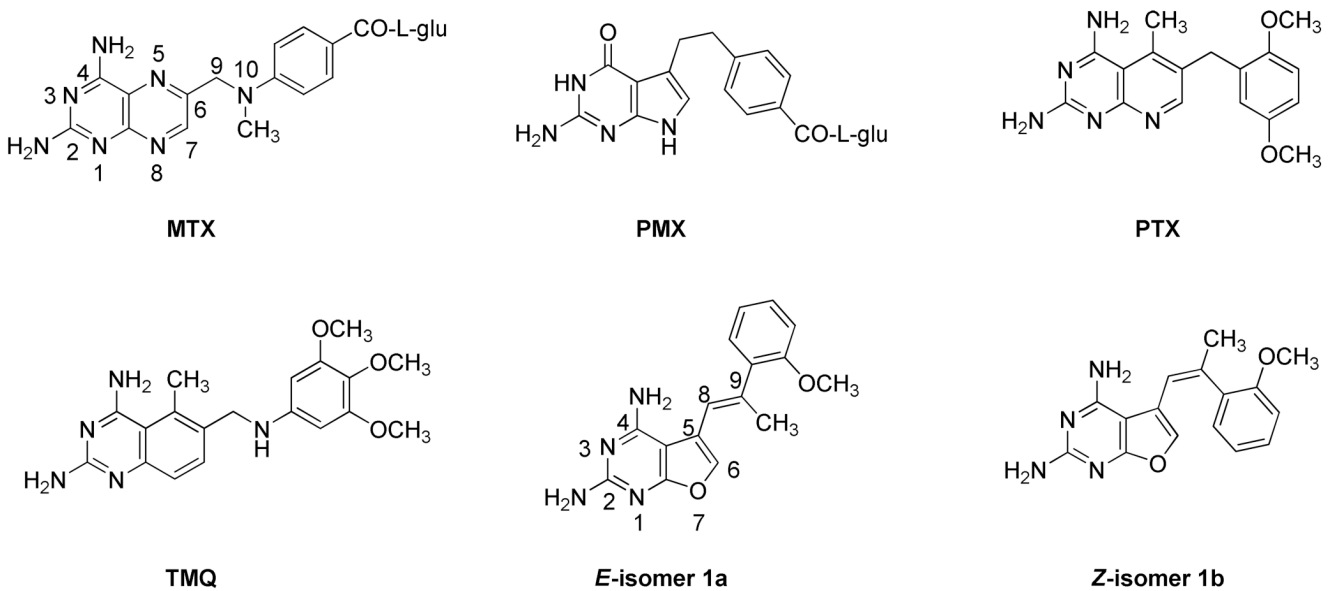
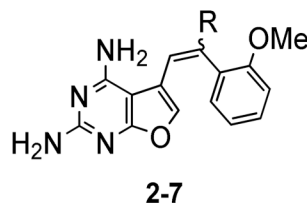


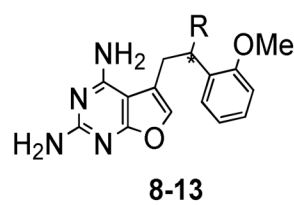
Figure 1.
Structures of small molecule inhibitors of RTKs.

**Figure 2.**

Structures of antifolates MTX, PMX, PTX, TMQ and E- and Z-isomers **1a** and **1b**.

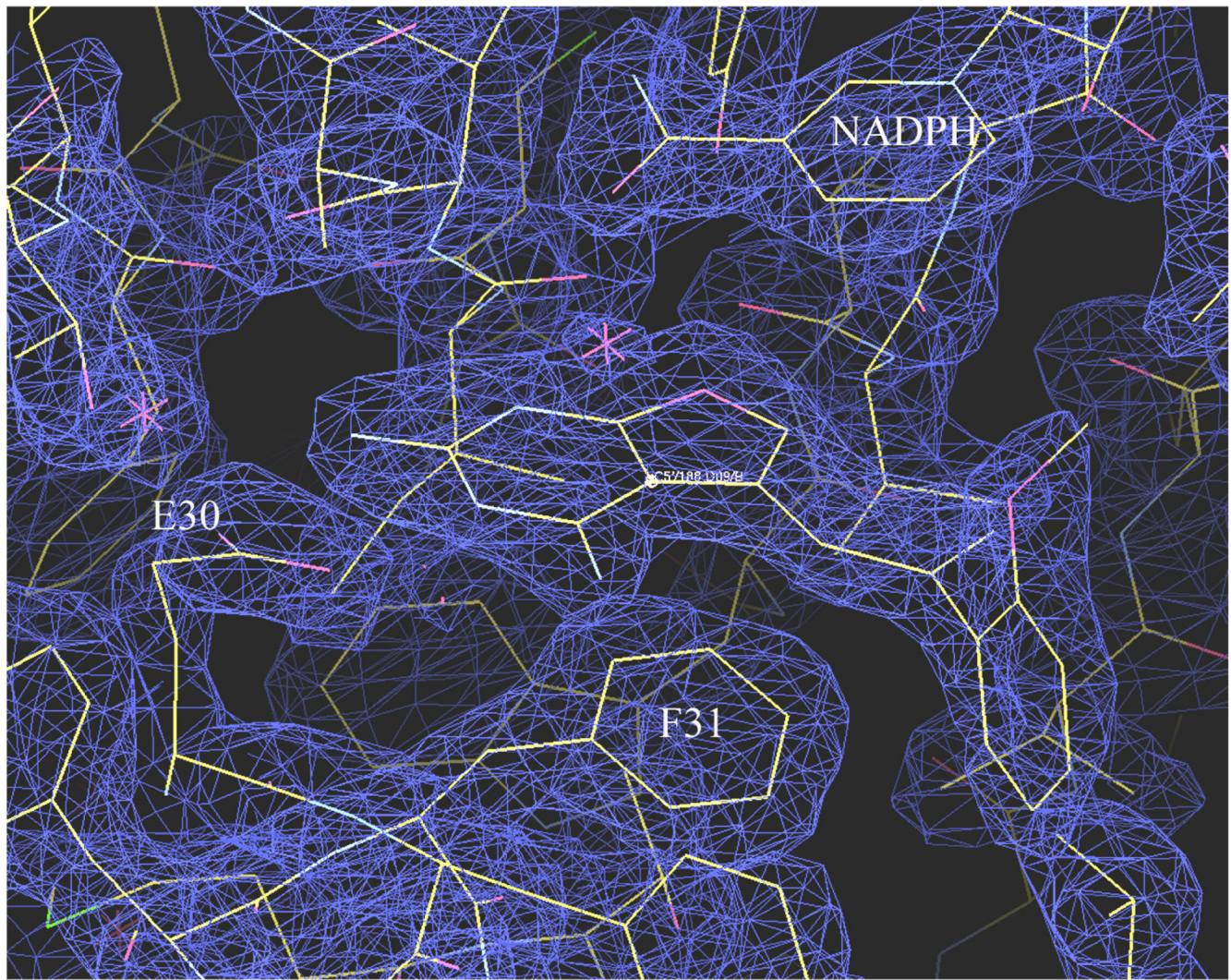


- 2. R = Propyl
- 3. R = Isopropyl
- 4. R = Cyclopropyl
- 5. R = Butyl
- 6. R = Isobutyl
- 7. R = sec-butyl

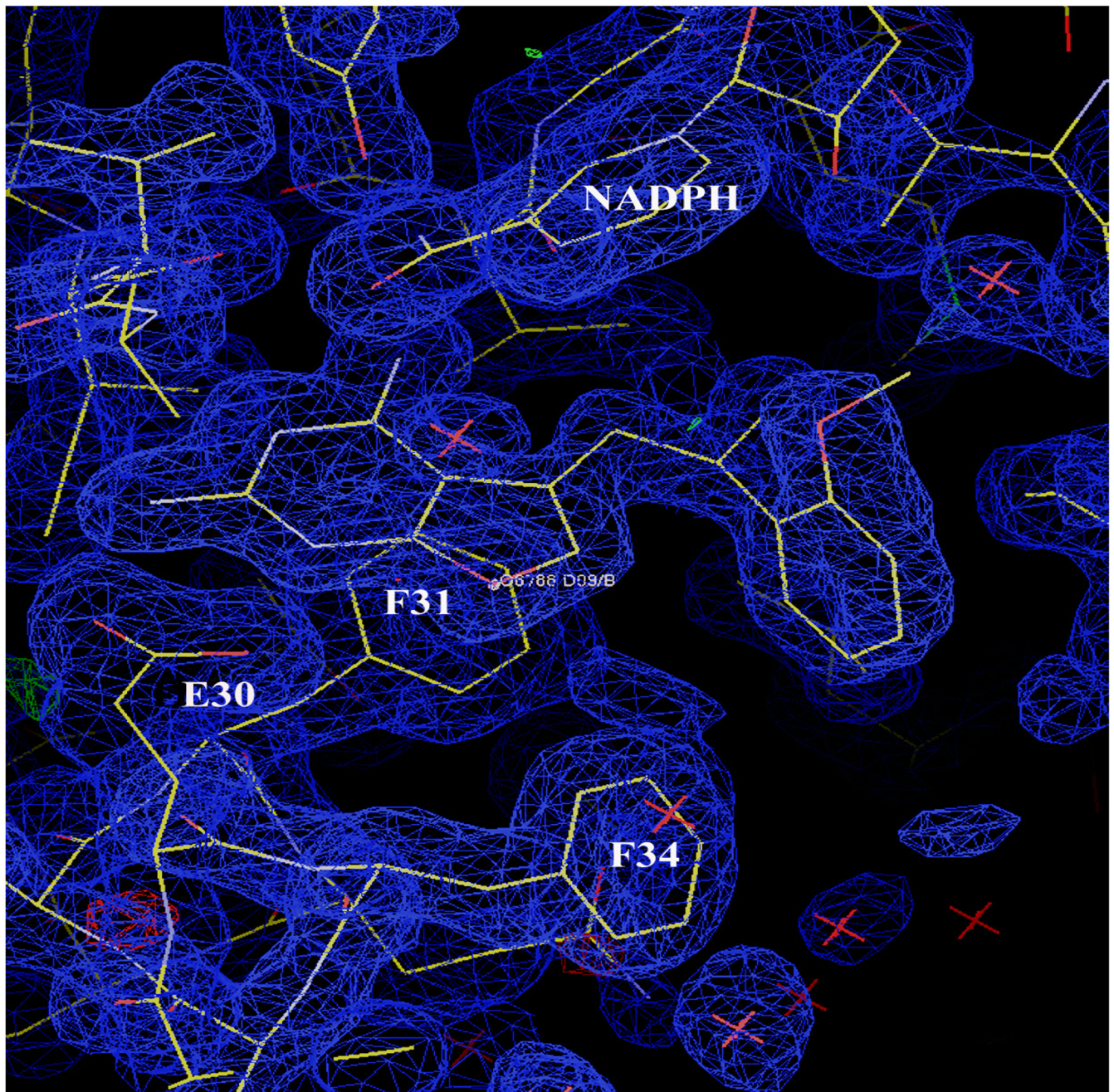


- 8. R = Propyl
- 9. R = Isopropyl
- 10. R = Cyclopropyl
- 11. R = Butyl
- 12. R = Isobutyl
- 13. R = sec-butyl

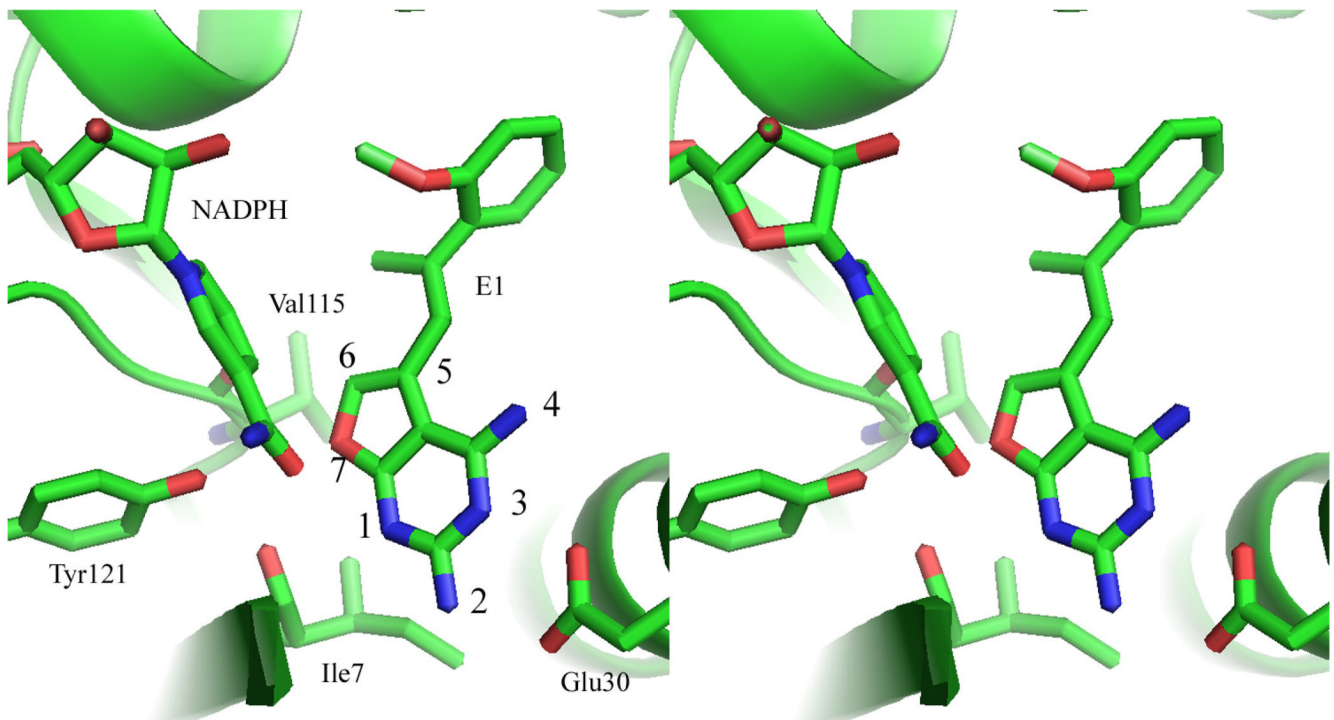
Figure 3.
Target compounds.

**Figure 4.**

View of the 2Fo-Fc difference density map for mDHFR-NADPH-**1a**, contoured at 1.2σ (blue). These data show a ternary complex with the E-isomer bound with a "flipped" furo[2,3-d] pyrimidine orientation with the furo oxygen of the furo[2,3-d]pyrimidine occupying the position of the 4-amino group of antifolates MTX, PTX etc. The configuration about the double bond is E with the 2'-methoxyphenyl ring trans to the furo[2,3-d]pryimidine ring. The 2'- methoxyphenyl ring is tilted nearly 90 degrees from the rest of the structure.

**Figure 5.**

View of the 2Fo-Fc difference electron density map for mDHFR-NADPH-**1b**, contoured at 1.2 σ (blue). The red X represents water molecules. These data show a ternary complex with the inhibitor **1b** bound with a normal antifolate orientation with N1 and the 2-amino group interacting with Glu30 (E30 in Figure 4 and Figure 5). The configuration about the double bond is Z- with the 2'-methoxyphenyl ring cis to the furo[2,3-d]pyrimidine ring.

**Figure 6.**

PyMOL³³ stereoview of the active site of mDHFR ternary complex with NADPH and **1a** highlighting the contacts to the furo[2,3-*d*]pyrimidine ring oxygen. The closest contacts are with the carbonyl of Ile7 and the hydroxyl of Tyr121 and the nicotinamide group of NADPH. These data show that inhibitor **1a** binds with furo[2,3-*d*]pyrimidine ring flipped from the normal orientation observed for most 2,4-diaminopyrimidine inhibitors.

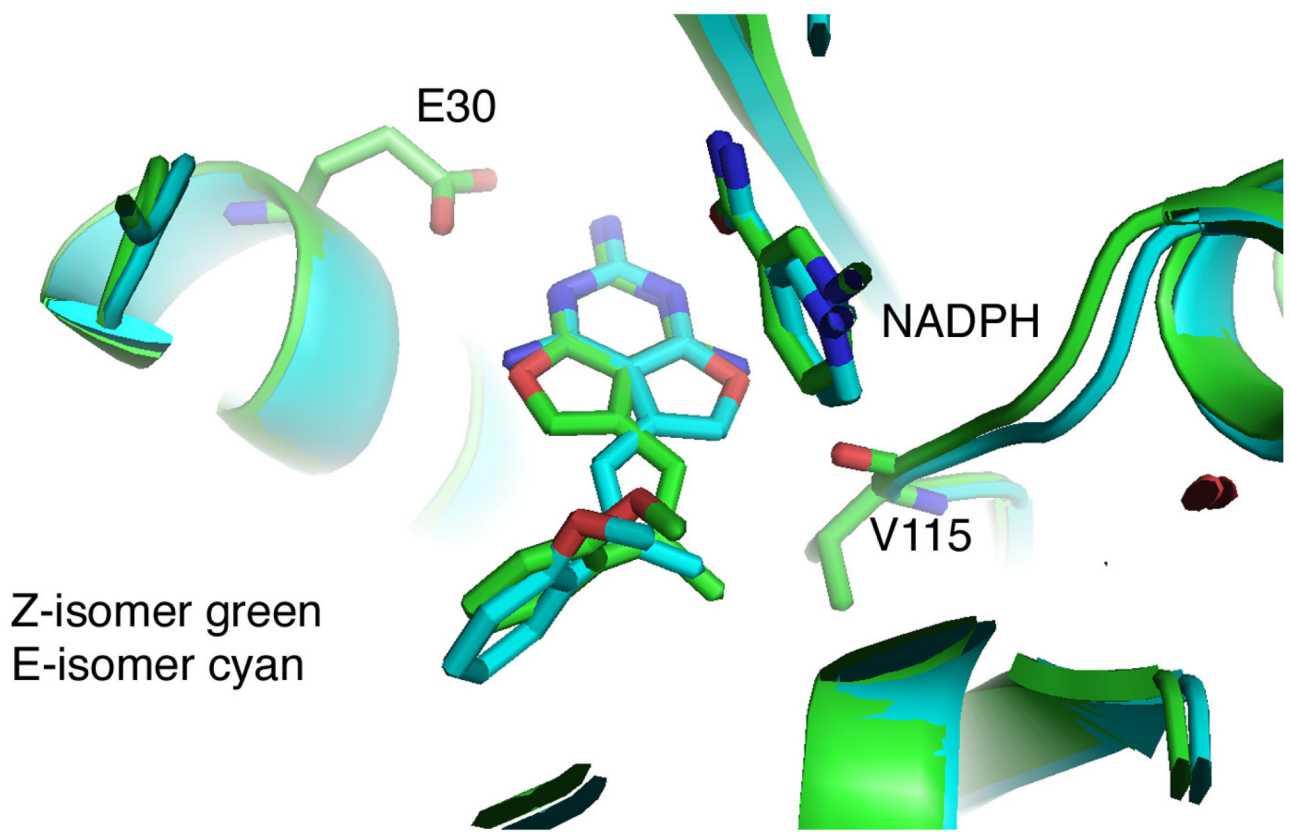


Figure 7.
(PyMOL)³³ Superimposition of **1a** (cyan) and **1b** (green) in the active site of mDHFR highlighting the different modes of binding for the E- and Z-isomers of the furo[2,3-*d*]pyrimidine analogs.

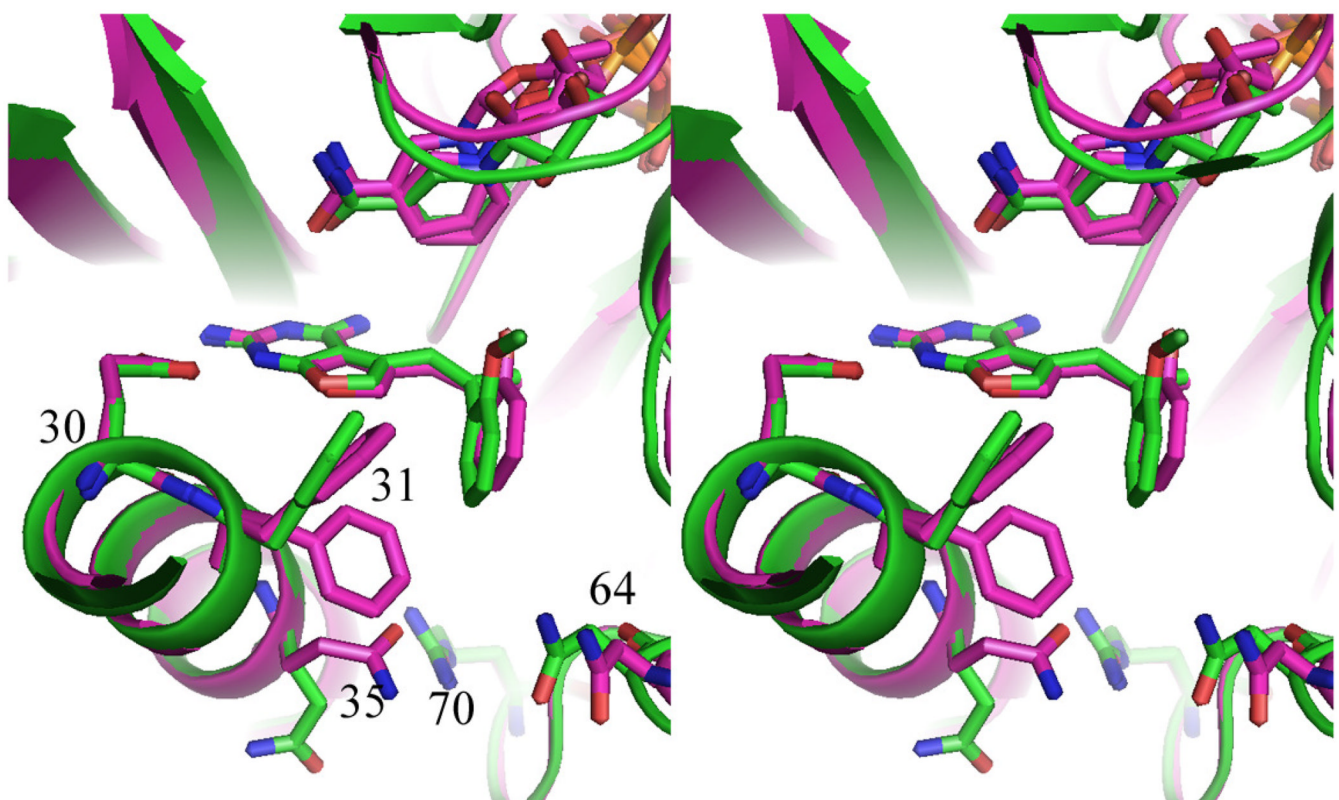
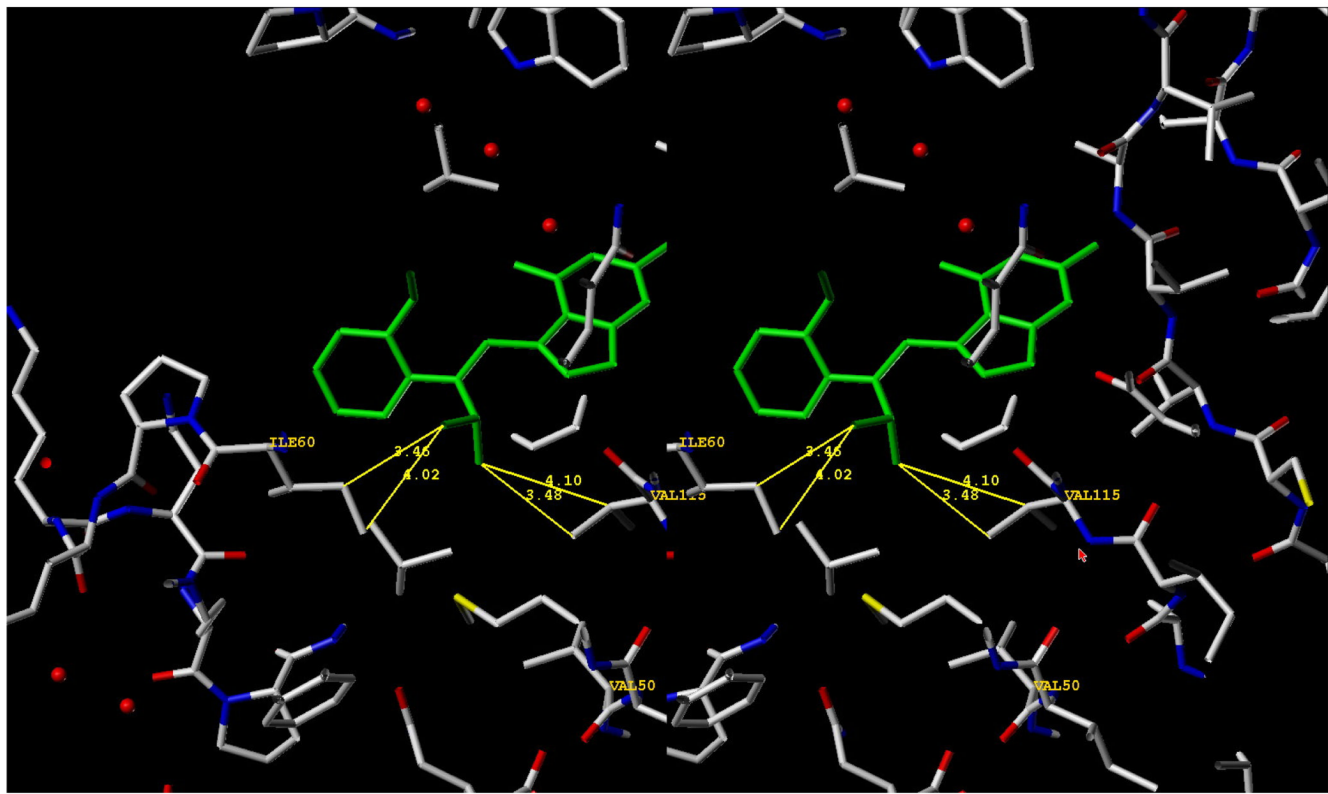


Figure 8.

(PyMol)³³ Superimposition of **1b** in human DHFR (green) and **1b** in mouse DHFR (violet) highlighting those residues in the active site that make contact with the inhibitor.

**Figure 9.**

Stereoview (SYBYL)³⁴ E-isomer of 3 (green) superimposed on the crystal structure of the E-isomer 1a (not shown) bound to the ternary complex of mouse DHFR and NADPH, showing contacts of the C9-isopropyl of 3 with residues Val115 and Ile60 of mouse DHFR.

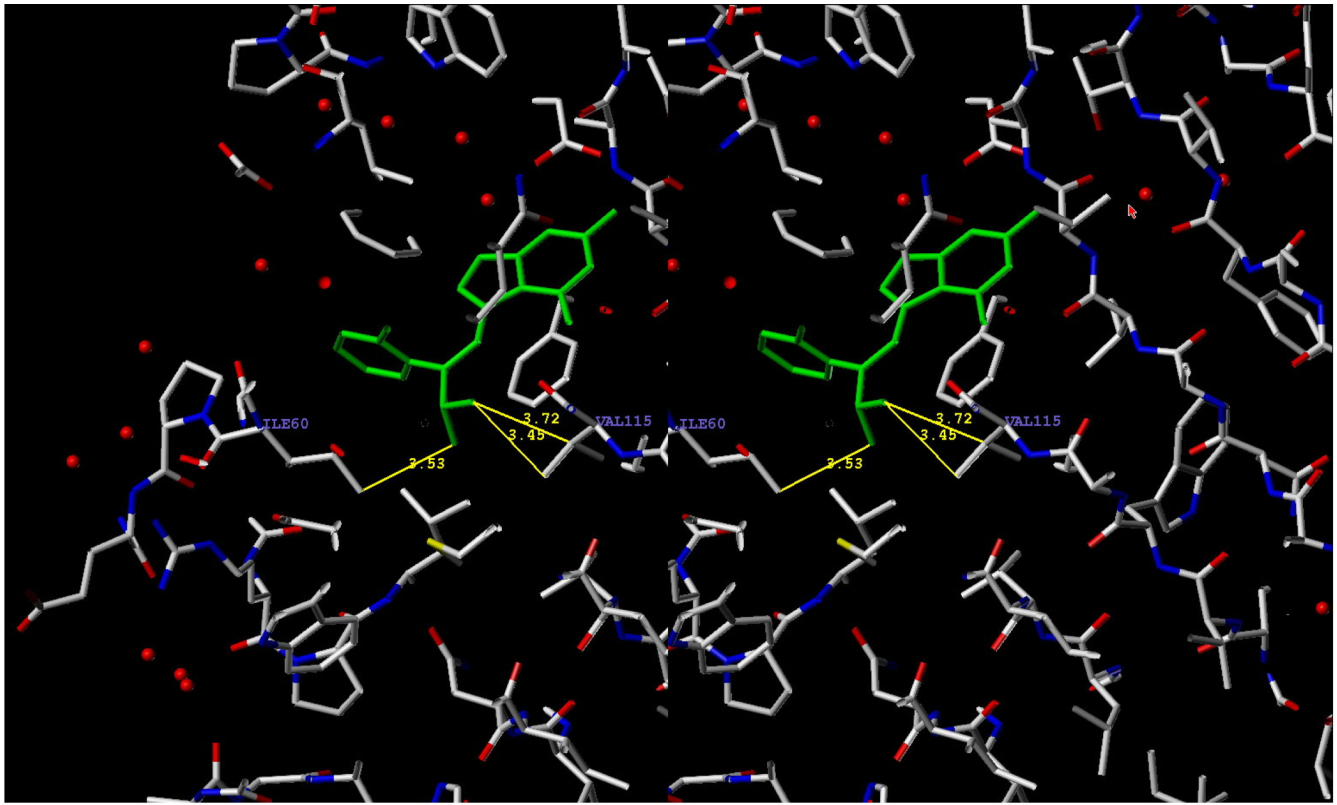
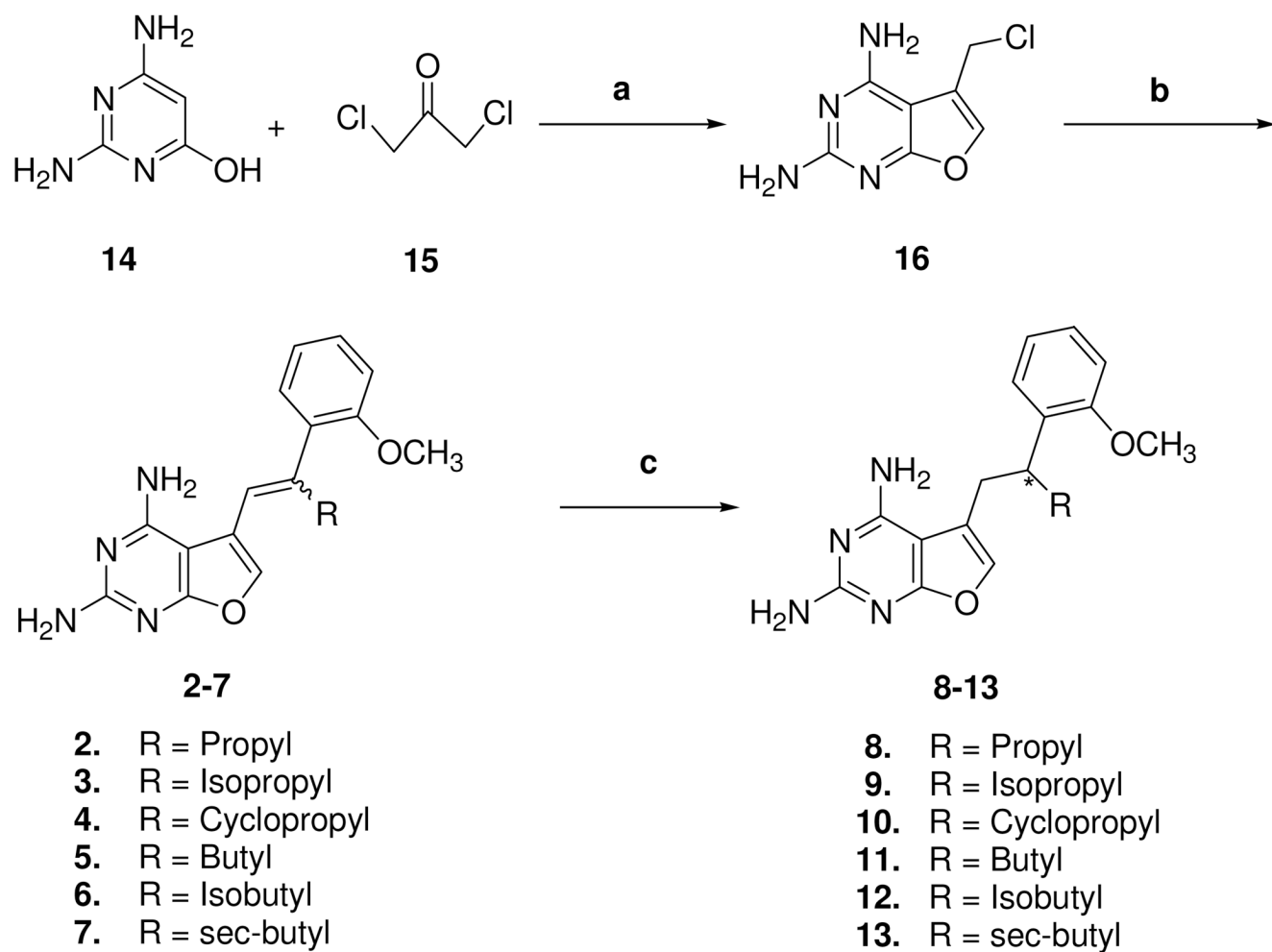


Figure 10.

Stereoview (SYBYL)³⁴ Z-isomer of compound **3** (green) superimposed on the crystal structure of the Z-isomer **1b** (not shown) bound to ternary complex of mDHFR and NADPH, showing contacts of the C9-isopropyl of **3** with residues Ile60 and Val115 of mDHFR.

**Scheme 1a.**

^a Reagents and conditions: (a) DMF, rt, 24 h; (b) NaH, tributylphosphine, alkyl-2-methoxyphenyl ketones, DMF, 60 °C, 3 h; (c) Pd/C, H₂, 55 psi, MeOH/CHCl₃.

Table 1

RTK inhibitory data and antiangiogenic activity IC₅₀ (μM)⁴³

Compd	E/Z ratio	EGFR kinase inhibition	V _{EGFR-2} kinase inhibition	PDGFR β kinase inhibition	A431 cytotoxicity	CAM angiogenesis inhibition
1a		<i>E</i> -isomer >50	12.8±1.6	10.3±1.2	ND	0.08±0.009
1b		<i>Z</i> -isomer >200	15.9	30.3	>250	17.8
2	2:1	160.3±20.1	88.2±14.3	17.8±2.4	>500	22.3±3.7
3	3:1	111.4±18.2	>200	>300	48.3±5.1	5.9±0.7
4	2:1	>200	>200	>500	9.5±1.4	5.0±0.6
5	3:2	529.3±65.2	>200	>500	>500	2.0±0.3
6	2:1	>200	>200	>500	18.6±3.0	16.7±1.8
7	3:2	>200	>200	>500	12.3±2.9	92.2±10.5
8		2.2±0.31	>200	>500	>500	11.7±2.3
9		18.2±2.2	118.0±16.3	5.0±0.9	>500	5.0±0.7
10		56.5±7.2	>200	13.7	>500	5.3±0.6
11		13.4±2.6	>200	>500	27.3±5.1	10.6±1.3
12		>500	>200	>500	106.3±17.3	9.3±0.8
13		>200	17.4±1.5	>500	12.6±1.4	5.6±0.61
17		0.2±0.03				
18	Semaxanib		2.4±0.2	6.2±0.3		0.03±0.004

Data represent a sample size of **7–16** from 2–3 separate experiments.

Table 2Inhibitory Concentration (IC_{50} μ M) against DHFR and selectivity ratios.

Compd	human DHFR	r^l DHFR	Mouse DHFR	Pc DHFR	r^l/Pc	T_g DHFR	r^l/T_g
1a	16.4	18.5	14.5	77	0.24	4.0	4.62
1b	1.9	10.19	3.9	30	0.34	3.94	2.58
2	12.2	15.2	7.92	37(30%)	ND	11.8	1.3
3	6.35	11.9	4.14	34(29%)	ND	7.5	1.59
4	10.2	10.34	4.64	22.2	0.5	4.6	2.2
5	33.3	29.9	31.2	25.9	1.2	30.3	1.0
6	86.5	43.9	51.9	52.6	0.8	24.9	1.8
7	8.64	9.64	4.2	55	0.2	5.7	1.7
8	25.9	30.8	162	42.5	0.72	30	1.03
9	5.09	12.6	3.2	53.6	0.24	7	1.80
10	5.01	10.1	3.7	12.5(12%)	ND	4.44	2.3
11	93.9	46.7	187	30.9	1.51	19.6	2.38
12	62.7	39.3	35.4	40	0.98	22.2	1.45
13	42.1	34.5	44.5	45.1	0.76	15.4	2.23

All assays contained 117 μ M (saturating concentration) NADPH and saturating concentrations of DHFA, optimized for each enzyme. Final DHFA concentrations in the assays were as follows: human DHFR 18 μ M; rat liver DHFR 90 μ M; mouse DHFR 18 μ M; Pc and Tg DHFR 90 μ M.

Table 3

Characterization of isomer and analog interactions with mammalian DHFR.

Compound	Mouse DHFR μM Ki	Human DHFR μM Ki	Rat liver DHFR μM Ki
1a	0.16 \pm 0.4 (n=5)	1.6 \pm 0.5 (n=3)	4.6 \pm 0.1 (n=3)
1b	0.062 \pm 0.01 (n=4)	0.5 \pm 0.26 (n=2)	1.1
1a+1b	0.092 \pm 0.005 (n=2)	0.5	1.4
2	0.14	1.6	1.6
3	0.07	0.83	1.3
4	0.08	1.3	1.1
5	0.55	4.3	3.2
6	0.91	11	4.7
7	0.07	1.1	1.0
8	2.8	2.5	3.3
9	0.06	0.77	1.4
10	0.06	0.65	1.1
11	3.3	12	5.0
12	0.62	5.3	4.2
13	0.78	4.6	4.0
TMP	0.5	4.9 \pm 0.7 (n=4)	14.3 \pm 1.4 (n=6)
MTX	0.000003 \pm 0.0000001 (n=2)	0.000077 \pm 0.000017 (n=10)	0.000073 \pm 0.000006 (n=4)

The Ki values were calculated as described, based on competitive inhibition except for MTX which acted as a tight binding pseudo-irreversible inhibitor. Values in the table that appear as single values represent Ki values determined from a single, full dose response curve; for others, the n value represents the independent experiments and the values are means \pm SEM.

Table 4

Crystal and Refinement Parameters for the E- and Z-isomers of 5-[2-(2-methoxyphenyl)prop-1-en-1-yl]furo[2,3-*d*]pyrimidine-2,4-diamines **1a** and **1b** as a NADPH ternary complex with mouse DHFR and for the E isomer **1a** with human DHFR.

Inhibitor	E-isomer 1a mDHFR	Z-isomer 1b mDHFR	E-isomer 1a hDHFR
Space Group	P21	P21	P212121
Lattice	41.43 61.01 43.22 $\beta = 117.79$	41.64 61.15 43.56 $\beta = 117.33$	39.91 57.48 74.97
PDB Entry	3d7y	3d7x	
Data Collection	Overall	Raxis IV	
Data collection	21.85	2.05	
Low resolution limit	2.10	2.05	
High resolution limit	0.063	0.320	
Rmerge	0.063	0.320	
Total number of observations	29811	2138	
Total number unique	10812	773	
Mean(I)/sd(I)	14.6	2.6	
Completeness	94.8	92.8	
Multiplicity	2.8	2.8	
R factor (%)	16.9	16.9	
R free weighted	24.7	24.7	
Protein atoms	1553	1553	
Water molecules	133	133	
Ramachandran (Procheck)	89.9	89.9	
B factor (protein average)	31.4	31.4	
Rms bonds	0.24	0.24	
Rms angles	2.60	2.60	
Rms chiral	0.17	0.17	
Overall		Raxis IV	
		17.82	
		1.64	
		0.074	
		28759	
		2236	
		24297	
		788	
		14.6	
		98.5	
		2.5	
		19.6	
		2.5	
		1.8	
		95.3	
		1.8	
		95.3	
		2.5	
		9.8	
		26.0	
		24.2	
		1553	
		1557	
		185	
		90.6	
		91.8	
		33.8	
		0.14	
		1.84	
		0.12	
		0.13	
		1.81	
		0.13	
Outer Shell			Outer Shell
		1.60	
		1.60	
		0.396	
		2236	
		24297	
		788	
		1.8	
		95.3	
		1.8	
		9.8	
		26.0	
		31.9	
		1557	
		64	
		91.8	
		33.8	
		0.14	
		1.84	
		0.12	
		0.13	
		1.81	
		0.13	

Table 5

Kinetic characterization of mammalian DHFRs

Kinetic parameter	Mouse DHFR	Human DHFR	Rat liver DHFR
K_m DHFA, μM	0.3 ± 0.05 (n=2)	2.7 ± 0.5 (n=4)	10.8 ± 3.4 (n=4)
K_m NADPH, μM	2.42 ± 0.05 (n=2)	4.0 ± 1.8 (n=2)	23 (ref)
K_{cat} , s^{-1}	29 ± 5 (n=4)	40 ± 2 (n=8)	